Supporting Online Material for

Coupled, Circumferential Motions of the Cell Wall Synthesis Machinery and MreB Filaments in *B. subtilis.*

Ethan C. Garner, Remi Bernard, Wenqin Wang, Xiaowei Zhuang, David Z. Rudner, Tim Mitchison

Correspondence to: ethan_garner@hms.harvard.edu

This PDF file includes:

Materials and Methods

SOM Text

Figs. S1 to S17

Captions for Movies S1 to S13D

Tables S1 to S5

Other Supporting Online Material for this manuscript includes the following:

Movies S1 to S13D, available at http://mitchison.med.harvard.edu/cellwall/

Materials and Methods

Culture growth. Unless otherwise noted, all cultures were prepared using standard conditions. Strains were streaked from freezer stocks onto LB plates containing the appropriate antibiotic. Single colonies from these plates were inoculated into CH medium, serially diluted, and grown overnight at 22˚C. The following day, mid-exponential cultures (OD600 0.2-0.6) were used as inoculums for 15ml cultures in 250ml beveled flasks. The starting OD600 was 0.05. These starter cultures were then serially diluted into flasks with the same medium and inducer to provide a series of cultures in exponential phase. Unless otherwise noted, all growth was done at 37˚C.

Imaging setup. All imaging with the exception of the particle tracking was done with an inverted spinning disk confocal microscope. We used 24x60mm coverslips as the imaging support as well as the coverslip itself. Samples were pelleted in a tabletop centrifuge at 8Krpm for 2 min. After removal of the supernatant, 4 µl of the concentrated culture was spotted onto the 24x60mm coverslip. Then, a 22x22 mm wide, 1.5mm thick agar pad was laid on top of the bacteria. This long coverslip/pad arrangement was placed slide onto the scope in a custom milled stage plate, with the pad facing upwards. The upper face of the pad was exposed to air, allowing adequate oxygen for *Bacillus* growth. Moreover, the thickness of the pad allowed the sample to remain hydrated for over an hour. This open-air configuration also allows for the addition of drugs to the pads.

Imaging – Spinning disk confocal. All imaging (other than particle tracking and TIRF) was done on a Nikon TE2000 microscope equipped with a Yokogawa CSU-10 spinning disk, PerfectFocus, a plan Apo 1.4 100x objective, and a Andor Ixon DU897-E camera equipped with tube lens to give an effective pixel size of 109nm. As noted below in Supplemental Text, significant phototoxicity can result from sustained imaging of the MreB paralogs, resulting in the slowing or stopping of MreB motion. Accordingly, we used low laser illumination and short exposure times (150-300ms).

Imaging – Particle tracking with Total Internal Reflection Microscopy. All imaging for the particle tracking experiments was conducted on a Nikon TI equipped with a 100X 1.49 TIRF objective and a Hamamatsu ImagEM C-9100-13 EM-CCD camera (effective pixel size of 160nm). For all movies, we used streaming acquisitions of 0.3 seconds, and analyzed the first 300 frames (100 seconds) of the movie. Any movies that displayed drift were discarded.

Depletions. Experiments where the dynamics of GFP-Mbl were examined during the depletion of RodA, RodZ, or Pbp2A were performed as follows. These strains contain a xylose-inducible GFP-Mbl fusion integrated at the non-essential locus *amyE*, and IPTG-inducible RodA (BRB728) or RodZ (BRB729) at the native locus. Similarly, Pbp2A was depleted in a strain with an IPTG-inducible Pbp2A fusion at the native locus with the redundant transpeptidase PbpH deleted (strain BRB785). These strains were grown overnight in the presence of 2mM IPTG, and then inoculated (at an OD600 of 0.05) into CH media containing 2mM IPTG, 0.015% xylose, and 20mM $MgCl_2$ to stabilize the cells against lysis. After these cultures reached an OD600 of 0.6, cells were spun down in in a tabletop centrifuge, washed 3 times in CH media lacking IPTG, and resuspended the same media as above lacking IPTG. Confocal image sequences were taken at the indicated time points using our standard imaging approach with agar pads containing 20mM $MgCl_2$.

Antibiotic treatments. Antibiotic stocks were created in water (or DMSO for vancomycin) at 50 or 80 mg/ml, and serially diluted 10-fold into the same medium. In all cases where DMSO was the solvent for the antibiotic, DMSO controls were conducted. Equivalent levels of DMSO alone had no effect on MreB motion. Most antibiotic studies were conducted using the spinning disk confocal. Actively growing cultures were spun down for 2 minutes in a tabletop centrifuge, and an initial image stack was acquired to ensure that the illumination conditions were not perturbing dynamics over the imaging interval (60 frames or longer). A new field of bacteria was then identified via brightfield. Following this, 2µl of antibiotics were added to the top of the 600µl (22mm x 22mm x 1.5mm) pad, and image acquisition initiated. For the kymographs in Fig. 2B and movies S6A,B,D we used lower concentrations of antibiotics and thick (1.5mM) agar pads, providing a time interval to demonstrate

the contrast between the periods of motion and frozen filaments. The "immediate freezing" experiments in movie S6C were conducted in a similar manner as described above with the following changes: 1) the antibiotics were added after frame 20 rather than the start of imaging, and 2) the agar pads were made very thin, created by spotting melted CH+2% agar onto a coverslip, and then placing a coverslip on top of this and pressing down. For treatments on the thin pads, we diluted our DMSO antibiotic stocks (1:1000) into water. Antibiotic treatments of cells in solution for dose experiments (movies S7 and S8) were carried out in a similar manner, where 1 ml of bacteria was removed from exponential phase culture, and 1-10µl of antibiotic stock added to the solution to achieve the desired final concentration. The tube was shaken for 2 minutes, and then 4 µl of the culture was spotted onto a coverslip, covered with an agar pad, and immediately imaged. This preparation took no more than 2 minutes once the bacteria were removed from the tube.

Image Processing. All image processing and movie construction was done in NIH ImageJ. Particle tracking movies were not altered in any manner, save contrast and size adjustments for display purposes. The only alteration to full field confocal images was contrast adjustments and background subtractions, although occasionally we used the plugin *Turboreg* (using a uniform rigid body transformation) to correct for pad drift, especially as pad drift often occurs when the antibiotics diffuse to the coverslip surface. To rotate cells into a uniform vertical orientation for kymograph analysis, cells were transformed using the ImageJ *rotate* command with bicubic interpolation. Kymographs were generated using the ImageJ *kymograph* command with a line width of 1. For display purposes, movies have been rescaled by 2-5x using the ImageJ scale command (no interpolation), so that the native antialiasing built into modern operating systems does not smooth the native pixels during display.

Growth, expression conditions, and microscopy for particle tracking.

Slide preparation. To remove background fluorescence due to impurities on the glass, coverslips were cleaned for TIRF imaging before use. Coverslips were sonicated in 1M KOH for 15 minutes, followed by extensive washing with ddH20. Coverslips were then sonicated in 100% ethanol, followed by 3 washes in 100% ethanol. These were stored in ethanol, and the ethanol evaporated for 15 minutes before use.

Imaging. Samples were prepared as above, where cultures were grown at 37˚C or 30˚C in a shaking water bath, and 1 ml of cells spun down in a tabletop centrifuge, resuspended in CH medium, and 4µl of resuspended cells placed onto the coverslip. Then, a 2% agar pad made with CH media was placed upon the cells, and the cells imaged via TIRF with illumination with a 491 laser. Brightfield image stacks were acquired before and after TIRF acquisitions for segmenting the outside of the cells. Slides were imaged at room temperature, and new slides made after 30 minutes.

MreB paralogs - Merodiploids. Particle tracking of GFP-MreB, GFP-Mbl, and GFP-MreBH paralogs was done using the xylose-inducible merodiploid strains BDR2436, BDR2437, BDR2438, respectively. These fusion proteins were induced with either very low xylose (0.3-3µM), or no xylose addition, as the leakiness of the PxylA promoter is often sufficient to provide diffraction-limited foci. We also found that growth temperature affects the expression levels of these strains, where cells grown with no addition of xylose at 37˚C have higher levels of background, whereas 30˚C yields better separated diffraction-limited foci and lower background. GFP-MreBH was the most difficult of the GFP MreB paralog fusions to titrate to low levels using merodiploid strains. Analysis of multiple experiments demonstrated that there was no difference in velocity, angle, or α in samples of all three paralogs grown at either 30˚C or 37˚C, and we include both sets of data in the analysis.

MreB paralogs - Replacements. Particle tracking of GFP-MreB, GFP-Mbl, and GFP-MreBH paralogs as the only source in the cell was done using the xylose-inducible chromosomal replacement strains BRB795, BDR2436, BDR2435 respectively. These proteins were induced with 3.3-33uM xylose to provide diffraction-limited foci. Cells were grown overnight at 22C in CH medium containing 20mM $MgCl_2$, and the following morning cells were diluted in the same medium with the appropriate xylose

concentration, serially diluted, and grown at 37˚C. Imaging was done as above except the agar pads were made with CH medium containing 20mM $MgCl_2$. Cells expressing low levels of MreBH display no apparent growth or shape defect (Fig. S4), but were imaged with pads containing 20mM $MgCl_2$ for consistency.

Mbl merodiploid in the absence of MreB. Particle tracking of strain BDR2461 (ΔmreB, amyE::PxlyA-gfp-mbl (spec)) was conducted in the same manner as above in "MreB paralogs - replacements", except the cells were grown in the presence of 33μM xylose.

GFP-MreC and GFP-MreD - Replacements. Particle tracking of GFP-MreC and GFP-MreD was done from xylose-inducible promoter fusions to these proteins (BDR2447 and BDR2448), which are the only copy of these proteins in the cell. Expression of these proteins at high levels (10mM xylose), where cells display a normal morphology, leads to rapidly diffusing signal not trackable via Gaussian fitting. To yield trackable diffraction-limited foci, we initially grew these cells in 10mM xylose, then shift the cells into lower induction conditions (0.5-1mM xylose), while stabilizing the cells against lysis using 20mM $MgCl_2$. As the cells gradually widen and become ovoid, diffraction-limited foci become observable that can be tracked with Gaussian fitting (movies S10A,B). These depletion conditions ultimately led to amorphous cells. Accordingly, movies were taken during the initial stages of depletion while cells still displayed a rod shape (Fig. S5). Cells were grown overnight at 22˚C in CH medium containing 20mM $MgCl_2$ and 10mM xylose, and the following morning mid-exponential cells were diluted in the same medium with the appropriate xylose concentration, serially diluted, and grown at 37˚C. Imaging was done as above except the agar pads were made with CH medium containing 20mM $MgCl_2$.

GFP-Pbp2A - Replacement. Particle tracking of GFP-Pbp2A was done using a xylose-inducible promoter fusion (strain BDR2444). As *pbp2A* is genetically redundant with *pbpH*, the levels of Pbp2A could be reduced without significant change in cellular morphology (Fig. S5). Accordingly, we did not use high concentrations of $MgCl_2$ when imagine GFP-Ppb2A. We found that the best induction levels to generate single foci were 50μM xylose. We note that if Pbp2A was initially induced from a state of no expression, the first culture inoculated from the overnights displayed a diffusive population of molecules during the first few generations. After ~2 hours of growth this shifted to a predominantly axially moving population, and every successive culture grown from this series displayed axially moving foci as the predominant phenotype (we tested this out to culture #5, from a 1:16 serially diluted culture series). Cells were grown overnight at 22˚C without inducer, and the next morning cells were diluted into CH medium with 50μM xylose, grown at 37˚C and imaged as above.

GFP-MreC, GFP-MreD, GFP-PBP2A - Merodiploids. Particle tracking of GFP-MreC, GFP-MreD, and GFP-Pbp2A paralogs as merodiploids was done using the xylose-inducible strains BRB690, BRB692, BRB684 respectively, where xylose inducible GFP-fusions to these genes was integrated at the non-essential locus *yvbJ.* These fusions were induced with 25-50uM xylose to yield diffraction-limited foci. Cells were grown overnight at 22˚C in CH medium, and the following morning cells were diluted into media with xylose, serially diluted (1:16) and grown at 37˚C. As before, these cells were imaged after 2 hours of growth. These conditions yield directionally moving foci, but as noted in the main text, these cells also contain large numbers of foci that rapidly diffuse within the membrane (movie S11). These rapidly-moving diffusive foci can interfere with the Gaussian fitting and tracking of the slow-moving directional foci (due to collisions), so a large number of movies must be taken in order to gain adequate statistics of well-fit traces.

Particle Tracking – Imaging, Gaussian Fitting, and tracking.

Particle tracking and image rendering of tracking was carried out using a home-written software in Microsoft Visual C++, normally utilized for the centroid assignment of STORM/PALM data (*1, 2*). Individual fluorescent peaks in each image frame were identified and fitted with a 2-dimensional Gaussian function in a 0.8*0.8 micron^2 vicinity to determine their precise positions as described previously (*1, 2*). Particle trajectories were then established by connecting fluorescent peaks in

consecutive frames. Two peaks in two consecutive frames are eligible to be connected only if their distance is smaller than 0.7 pixels, or 112 nm. In the case of multiple eligible connections for a given peak, a simple full-frame optimization was implemented to minimize all the pair-wise distances between two frames. Traces were terminated if foci no longer satisfied the Gaussian criteria or intersected, and no joining or splitting of trajectories was used. Trajectories shorter than 8 frames were discarded during tracking, and only traces longer than 20 frames were used for analysis when noted. Identical identification and tracking parameters were used for all proteins, using parameters similar to those used for STORM localization of photoactivatible proteins.

Data analysis.

Segmenting of cell shape. We were able to determine a pixel-by-pixel outline of each chain of cells (hereafter referred to as "cell-chains" within this section of data analysis) by segmenting brightfield images using MicrobeTracker (*3*) a software suite developed by the Emonet and Jacobs-Wagner labs. This software returns a 2D-coordinate mesh, representing the left and right side of the cell-chain, where the zero points and maximum values indicates the ends of each cell-chain. We used this mesh to determine the local midline, by determining the midpoint between these points.

Data processing and analysis – general considerations. All data processing and analysis were done in MATLAB using custom-written code. We combined the tracking data from the above tracking software with the data from MicrobeTracker. The tracking software returns the X and Y positions of the traces, their lifetime, their frames, and also the height, background, and width of the Gaussian peaks. MicrobeTracker returns a numbered list of cells with corresponding 2D meshes, which we joined into polygons. We determined what cell-chain (from MicrobeTracker) each trace fell into by determining the average position of each trace, then using *inpolygon* to search the cell-chain list. Traces were then assigned a value corresponding to each cell-chain. For all analysis, only traces that could be identified to be within a single cell-chain were considered.

Data processing and analysis – Angle of intersection. To find the angle at which these traces crossed the cells, we needed to determine two trajectories, first the line of the trace itself, and then the local midline of the cell-chain. We found the local midline of the cell-chain by searching for the nearest point of the midline (determined above) from the average position of each trace. This nearest midline point was extended by one point on either side, and these three points fit to a line. Traces from the particle tracking were then fit to a straight line, and then r^2 was used to assess fit quality. The angle of intersection between these two lines was then determined. As these angles are given a sign indicating direction (-90, 90) relative to the midline, we used the absolute value of these angles for the histograms in Fig. 4C and S11.

Data processing and analysis – Relative Orientation of traces as a function of distance (Fig 4D). We used the signed nature of our angles to determine whether proximal traces were going in the same direction across the cell width, as the sign of these angles denotes their trajectory relative to the local midline. Because the angles of the trajectories that cross the midline are Gaussian distributed around 90 (or -90), we binned all negative angles to be -90, and all positive angles to be 90. We then determined the distances between all pairs of angles within each cell, and calculated the fraction of angles moving in the same (90,90 or -90 -90) orientation in 1-pixel (160nm) increments. For this analysis we used the tracking data from the merodiploid-expressed Mbl, and replacement-expressed MreC, MreD, and Pbp2A, as these expression conditions yield the most dense tracking results, and hence allowed us to examine closely spaced trajectories. We used all traces in cells that could be fit to a line with an $r^2 > 0.5$. A similar analysis, looking at the angular correlation as a function of distance, using either binned (90,-90) or native angle values yielded similar results, with weak or no correlation at all length scales (Data not shown).

Data processing and analysis – Determination of velocity and α. For each trace, a series of parameters was determined. First, Mean Squared Displacement vs. time delay (MSD vs. t) was computed for all traces. We fit these curves to the quadratic $MSD(t)=4D(t)+(Vt)^2$, using nonlinear

least squares fitting. As these curves often diverge at long time values, we fit the first 80% of the data points. We determined α by fitting a straight line to log(MSD(t)) vs. log(t). The fit to this line was evaluated by determining the r^2 value, and these criteria used to evaluate particles that moved in a consistent manner during their lifetime.

Data processing and analysis - Selection of data for analysis. Data used in this study was subject to a few simple criteria for analysis. As noted above, only traces that were determined to be within cells were used, and to maintain consistency in data sets between the calculations of velocity from MSD(t) vs (t) and the windowed velocity of 20 frames, only traces longer than 20 frames were analyzed for all data. This group of "All traces" represents the subset of data shown in Fig. S7.

To determine accurate values for our velocities and α, we only examined particles that moved in a consistent manner and direction during their lifetime by evaluating those that had good linear fits (r^2>0.95) to the to the log (MSD(t)) vs log (t) plot. This represents the subset of "well fit" data shown in Figs. 4A, 4B, S9, and S12. We also present the same analysis with no exclusion of traces in Fig. S7.

For the analysis of angles particles move across the midline, we used the subset of traces found within cells with lifetimes above 20 frames and determined how well we could fit these traces to a line by determining the r^2 to a linear fit, and we present histograms based on cutoffs of r^2<0.5 and 0.7. This represents the subset of data shown in Figs. 4C and S11. While we did not filter this data to exclude any of the "low velocity" or badly fit log (MSD(t)) *vs*. log (t) particles, we find that evaluating the linearity of the trace itself largely excludes these populations, and these sets (the "well fit" + "high velocity" and "r^2 > 0.5 angle") largely overlap.

We note that equivalent analyses using only traces with lifetimes above 10 or 15 frames yielded similar mean values and distributions for velocity, angle, and α in both the "well fit" and "no fit" cases.

Data processing and analysis - Display of traces in raw tracking movies. The display of trajectories within movie S9A shows the raw tracking of particles above 8 frames in length, colored along their trajectory. No other filtering of data was used.

Data processing and analysis - Display of traces in figures. The display of the traces shown in Fig. 3 was conducted using a custom Matlab script, which combined the traces with the outlines and midlines of the cells. Traces that fit with an r^2> 0.5 are displayed, colored blue to red along their trajectory.

Plasmid construction

pRB089 [*yvbJ::PxylA-gfp-pbp2A (erm)*] was generated in a two-way ligation with an *XhoI-BamHI* fragment containing *pbp2A* (oligonucleotide primers oDR817 and oDR818 and PY79 genomic DNA as template) and pRB077 cut with *XhoI* and *BamHI*. The *pbp2A* gene sequenced using oRB161 and oRB082. pRB077 [*yvbJ::PxylA-gfp (erm)*] was generated in a two-way ligation with an *NheI-XhoI* PCR product containing *gfp* and an optimized RBS (oligonucleotide primers oRB074 and oRB075 and pKL147 (*4*) as template DNA) and pRB074 cut with *NheI* and *XhoI*. pRB074 [*yvbJ::PxylA (erm)*] was generated in a two-way ligation using an *EcoRI-BamHI* fragment containing the *PxylA* promoter and *xylR* (oligonucleotide primers oRB071 and oRB073 and pDR150 as DNA template) and pNS027 cut with *EcoRI* and *BamHI*. pDR150 [*amyE::PxylA (spec)*] is an ectopic integration vector containing the xylose-inducible promoter *PxylA* (D.Z.R., unpublished). pNS027 [*yvbJ::erm*] is an ectopic integration vector for double cross-over insertions into the nonessential *yvbJ* locus (Nora Sullivan and D.Z.R., unpublished).

pRB089 [*yvbJ::PxylA-gfp-mreB (erm)*] was generated in a two-way ligation with an *XhoI-BamHI* fragment containing *mreB* generated by PCR (oligonucleotide primers oRB085 and oRB086 and PY79 genomic DNA as template) and pRB077 cut with *XhoI* and *BamHI*. The *mreB* gene was sequenced using oligonucleotide primers oRB081, oRB082 and oRB161.

pRB091 [*yvbJ::PxylA-gfp-mreC (erm)*] was generated in a two-way ligation with an *XhoI-BamHI* fragment containing *mreC* generated by PCR (oligonucleotide primers oRB089 and oRB090 and PY79 genomic DNA as template) and pRB077 cut with *XhoI* and *BamHI*. The *mreC* gene was sequenced using oligonucleotide primer oRB161.

pRB092 [*yvbJ::PxylA-gfp-mreD (erm)*] was generated in a two-way ligation with an *XhoI-BamHI* fragment containing *mreD* generated by PCR (oligonucleotide primers oRB091 and oRB092 and PY79 genomic DNA as template) and pRB077 cut with *XhoI* and *BamHI*. The *mreD* gene was sequenced using oligonucleotide primer oRB161.

pRB095 [*rodZΩPspank-rodZ (cat)*] was generated in a two-way ligation using a *NheI-BamHI* PCR product containing the 5' end of *rodZ* (*yfmM)* (oligonucleotide primers oRB149 and oRB150 and PY79 genomic DNA as template) and pRB094 cut with *NheI* and *BamHI*. The *rodZ* fragment was sequenced using oligonucleotide oDR830. pRB094 [*Pspank (cat)*] was generated in a 3-way ligation with an *EcoRI-NheI* PCR product containing the *Pspank* promoter (oligonucleotide primers oRB157 and oRB158 and pDR110 as DNA template), an *NheI-HindIII* PCR product containing the *lacI* gene (oligonucleotide primers oRB159 and oRB160 and pDR110 as DNA template) and pER19 cut with *EcoRI* and *HindIII*. pDR110 [*amyE::Pspank (spec)*] is an ectopic integration vector containing the *Pspank* promoter and its regulatory elements (D.Z.R., unpublished). pER19 is a pUC19 derivative containing a *cat* cassette (*5*).

pRB096 [*rodAΩPspank-rodA (cat)*] was generated in a two-way ligation using an *NheI-BamHI* PCR product containing the 5' end of *rodA* (oligonucleotide primers oRB151 and oRB152 and PY79 genomic DNA as template) and pRB094 [*Pspank Ω (cat)*] cut with *NheI* and *BamHI*. The *rodA* fragment was sequenced using oligonucleotide oDR830.

pRB110 [*yhdG::Phyperspank-mreB^{D158A} (phleo)*] was generated by site-directed mutagenesis using oRB165 and pRB105. The construct was sequenced using oligonucleotides oDR829, oDR830 and oRB167. pRB105 [*yhdG::Phyperspank-mreB (phleo)*] was generated in a two-way ligation with a *HindIII-NheI* PCR product containing *mreB* and an optimized RBS (oligonucleotide primers oRB163 and oRB164 and PY79 genomic DNA as template) and pJW004 [*yhdG::Phyperspank (phleo)*] (*6*) cut with *HindIII* and *NheI*.

pRB111 [*yhdG::Phyperspank-mreB^{E136A} (phleo)*] was generated by site-directed mutagenesis using oRB182 and pRB105. The construct was sequenced using oligonucleotides oDR829, oDR830 and oRB167.

pRB112 [*yvbJ::PxylA-gfp-mreB ^{D158A} (erm)*] was generated by site-directed mutagenesis using oRB165 and pRB089. The construct was sequenced using oligonucleotides oRB081, oRB082, oRB161 and oRB167.

pRB113 [*yvbJ::PxylA-gfp-mreB ^{E136A} (erm)*] was generated by site-directed mutagenesis using oRB182 and pRB089. The construct was sequenced using oligonucleotides oRB081, oRB082, oRB161 and oRB167.

pRB115 [*yhdG::Pspank-pbpA (phleo)*] was generated in a two-way ligation with a *HindIII-SphI* PCR product containing *pbpA* and its RBS (oligonucleotide primers oRB176 and oRB177 and PY79 genomic DNA as template) and pRB114 cut with *HindIII* and *SphI*. pRB114 [*yhdG::Pspank (phleo)*] was generated in a two-way ligation with an EcoRI-BamHI fragment containing the *Pspank* promoter and *lacI* gene from pDR110 [*amyE::Pspank (spec*)] and pBB280 cut with *EcoRI* and *BamHI*. pBB280 [*yhdG*::*phleo*] is an ectopic integration vector for double cross-over insertions into the nonessential *yhdG* locus (Brianna Burton and D.Z.R., unpublished).

pRB117 [*yhdG::PxylA-mCherry-mreB (phleo)*] was generated in a two-way ligation with a *EcoRI-BamHI* fragment containing *PxylA-mCherry-mreB* from pRB108, and pBB280 [*yhdG*::*phleo*] cut with

EcoRI and *BamHI*. pRB108 [*yvbJ::PxylA-mCherry-mreB (erm)*] was generated in a two-way ligation with a *HindIII-XhoI* PCR product containing *mCherry* and the RBS from the *mreB* gene (oligonucleotide primers oRB173 and oRB174 and pDR201) as DNA template) and pRB089 cut with *HindIII* and *XhoI*. pDR201 [*mCherry*] contains a *B. subtilis* codon-optimized version of mCherry (D.Z.R., unpublished).

Supplemental Text

A. Directional motions of hydrolysis-deficient MreB mutants.

Previous work (*7*) suggested that a mutation in the phosphate-binding loop of MreB (specifically, D158A) changes the localization of GFP-MreB as well as abolishes its *in vivo* dynamics. This work also reported that the ectopic expression of unlabeled MreB(D158A) alters the localization and inhibits the dynamics of wild type GFP-MreB or GFP-Mbl. As our results indicate that the predominant force driving MreB motion is cell wall synthesis and not polymer dynamics, we reexamined the effects of mutations in MreB that impair ATP hydrolysis on its cellular dynamics.

We first examined the *in vivo* dynamics of GFP-MreB (D158A) using spinning disk confocal imaging. GFP fusions to this MreB mutant were reported to form irregular filaments that are no longer dynamic (*7*). We generated the identical mutant under xylose control and inserted it at an exogenous locus (strain BRB736). As shown in the first image sequence of movie S4, we also observed that this mutation alters GFP-MreB localization, as the signal appears to become more condensed, resulting in less homogenous GFP-MreB fluorescence throughout the cells. This distribution of filaments eventually results in bulged cells (Fig. S1A). However, in contrast to the previous report, we observed that these filaments still undergo axial dynamics, as small fragments and longer banded arcs move across the cell width. This is shown in movie S4 (first sequence) and movie S2B (far right), and represented by a kymograph in Fig. 1B (*far right*). Furthermore, kymograph analysis indicates that these mutant filaments move at similar rates (26nm/sec) to all three of the MreB paralogs (~22nm/sec, determined by kymograph, or ~20nm/sec determined by particle tracking via merodiploid expression.).

We wished to further confirm this finding with a second hydrolysis mutant. The D158A mutation in MreB maps to D154 in eukaryotic actin. Past work has suggested that D154 is involved in coordination of Mg^{2+}, a cofactor required for ATP hydrolysis (*8, 9*), but this mutation, while often used, has not yet been biochemically characterized in either actin or MreB. Therefore, to test if the hydrolysis state of MreB influences its cellular dynamics, we constructed a second strain containing a different mutation (E136A) based upon the structural homology in the catalytic sites of actin, MreB, and ParM. The E136 residue of MreB aligns with Q137 in actin and E138 in ParM. In actin, Q137 has been postulated to coordinate the catalytic water that makes a nucleophilic attack on the γ-phosphate of ATP (*8*). Supporting this prediction, the structurally superimposable residue in ParM, E148, has been shown to mediate ATP hydrolysis, as a ParM(E148A) mutation completely abolishes ATPase activity while allowing normal association dynamics in the ATP trapped state (*9*). Therefore, we constructed a strain with a GFP-MreB(E136A) mutant under xylose control, which, as above, was inserted at an ectopic locus (strain BRB770). Imaging of this strain (the second image sequence in movie S4) also shows that, similar to GFP-MreB(D158A), the filaments form a more condensed, sparse, and irregular arrangement, and also irregular cell morphology (Fig. S1B). Moreover, similar to the MreB(D158A) mutation, we also observed these filaments to undergo axial movements across the cell, as seen in movie S4 (second sequence) and Fig. S1C. As above, GFP-MreB(E136A) filaments also moved at similar rates (24nm/sec) to the MreB paralogs as determined by kymograph analysis. Together, these results indicate that fusions harboring 2 different hydrolysis-inhibiting mutations still undergo axial dynamics at the same rate as wild type polymer.

Defeu Soufo et al (*7*) report that the expression of unlabeled MreB(D158A) affects both the localization and dynamics of GFP-Mbl and GFP-MreB. Specifically, the GFP-labeled proteins lose their dynamic movement and become more banded along the cell length. We constructed similar strains, where MreB(D158A) was expressed from a strong IPTG-inducible promoter, and GFP-MreB (BRB755) or GFP-Mbl (BRB747) was expressed from a xylose-inducible promoter. As shown in the two last sequences of movie S4, we also observe that the expression of MreB(D158A) alters the localization of GFP-MreB, as the signal becomes more banded, running in axial stripes along the cell length. However, in contrast to previous work, close examination of our movies reveals axial motions within these banded patterns. This is most evident in areas with incomplete "rings", as a banded pattern obscures axial motion because there is no visual reference point to follow movement. Similar results were also obtained examining GFP-Mbl during expression of MreB-D158A (Data not shown).

The above experiments suggest that while the hydrolysis state of MreB affect its localization pattern, it does not affect the axial motions of the filaments, as we observe directed movement at rates similar to wild type GFP-MreB in the above strains. These results suggest that the nucleotide bound state of MreB does not affect its axial dynamics, although it does affect its ability to form regular cellular structures. If MreB is a treadmilling polymer, high levels of hydrolysis-deficient MreB should block treadmilling by inhibiting dissociation from the pointed, ADP-bound filament end. Furthermore, this should reduce overall free monomer levels, and hence reduce the overall dynamics of the filaments. As we observe that GFP-fusions to two different hydrolysis mutants of MreB still move across the cell at similar rates, we conclude that the cellular motion of the MreB paralogs in *B. subtilis* cannot be accounted for by treadmilling, in agreement with previous biochemical studies (*10*).

We cannot explain the discrepancies in our findings with those reported previously. We suspect they could be due to the time after induction of the mutant proteins or to the improvement in imaging approaches since the original study. Our imaging setup (a spinning disk confocal equipped with Nikon PerfectFocus and an Andor Ixon EMCCD camera) allowed us to maintain the exact focal plane for hours, and to resolve motion under weak signal conditions. The original study used an approach in which focal drift may have made it difficult to observe these filament dynamics.

B. Rapidity of antibiotic-induced freezing of motion.

The antibiotic-induced freezing of MreB paralog dynamics was a rapid process, and therefore, likely reflects a direct effect. The kymographs in Fig. 2B and the movies S6A,B, and D show a significant time-delay (~100-300 seconds) between the addition of antibiotics and cessation of movement. We note that these experiments have been conducted with concentrations of antibiotics and sufficiently thick agar pads (1.5mM) to provide a visual contrast between the phase of movement and the phase of frozen filaments. We know this lag is based upon the time it takes the drugs to diffuse though to the cells, as imaging of equimolar mixtures of antibiotics and similar molecular weight fluorescent dyes suggest that motion ceases as soon as the antibiotic diffuses to the bacteria at sufficient concentrations (Data not shown). When the concentration of the drugs is increased, or the thickness of the pads is reduced, the freezing of filament motion occurs at a significantly faster rate. To directly demonstrate the rapidity of antibiotic-induced freezing, we placed cells under paper-thin agar pads and evaluated the time required to stop GFP-Mbl motion following the addition of antibiotics. This is shown in movie S6C. In all cases, we added the

antibiotic in between frame 20 and 21. We observe that freezing occurs within 1 frame (10 seconds) at concentrations 100-fold above the MIC, and within 2-3 frames (20-30 seconds) at concentrations 10-fold above the MIC.

C. Particle tracking of diffraction limited foci.

The primary technique used in this paper is the Gaussian fitting of diffraction-limited foci. This approach allows for spatial localization of a point source of light beneath the diffraction limit down to nanometer accuracy. This technique is easy to implement, and we point the reader to the following references (*11-14*). A variety of software packages exist to both fit and track diffraction-limited foci, and we suggest the interested reader examine the *u-track* software package developed by the Danuser group (*15*).

D. Notes on imaging *B. subtilis* MreB.

We have observed that sustained, bright illumination of GFP fusions to the MreB paralogs results in significant phototoxicty, manifested by an apparent slowing, or even cessation of motion. We know this effect is specific to irradiation, as after brightly illuminated regions displayed an inhibition of filament motion, subsequent imaging of adjacent unilluminated areas on the same pad displayed filament movement at normal rates. We find that the use of spinning disk illumination, low excitation intensities, short exposure times, and the use of a EMCCD camera can minimize this phototoxicity effect, allowing time lapse experiments to be conducted for long intervals (~10 minutes with 10 second intervals) without observable slowing of motion. While these low illumination conditions result in less signal for each exposure, they are necessary so as not to perturb the dynamics of movement over long time intervals. To control for phototoxicity effects, all antibiotic experiments in this work were prefaced with an illumination only control, to ensure that the dynamics were not affected by irradiation over time, and the observed effects of the drugs were solely due to the pharmacological treatments. We note that TIRF illumination appears to yield the least phototoxicity of all imaging approaches, and constant illumination at low laser power can be used up to ~200 seconds without perturbing dynamics.

Supplemental Figures and Legends

S1A D158A MreB brightfield images

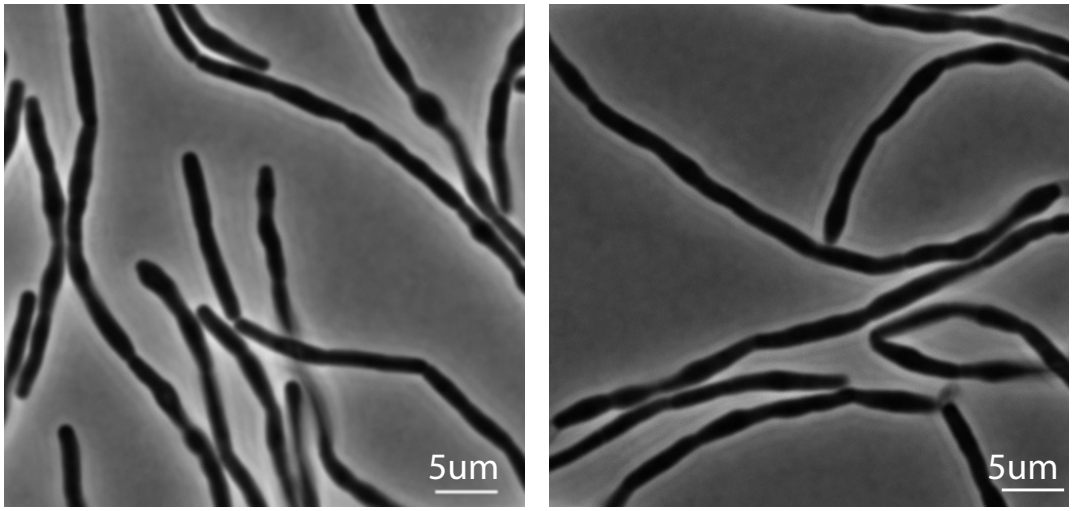

S1B E136A MreB brightfield images

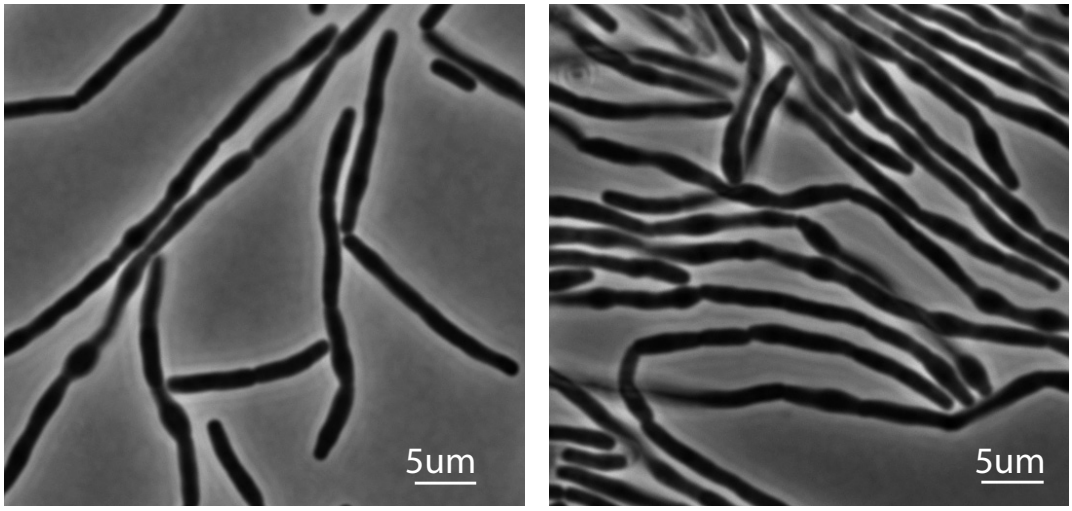

S1A,B – Expression of MreB hydrolysis mutants results in bulging cells. Brightfield images of cells expressing **(A)** GFP-MreB (E158A) (Strain BRB736) and **(B)** GFP-MreB (E136A) (Strain BRB770). Both strains were induced with 10mM xylose, grown in CH at 37°C, and imaged after 100 minutes.

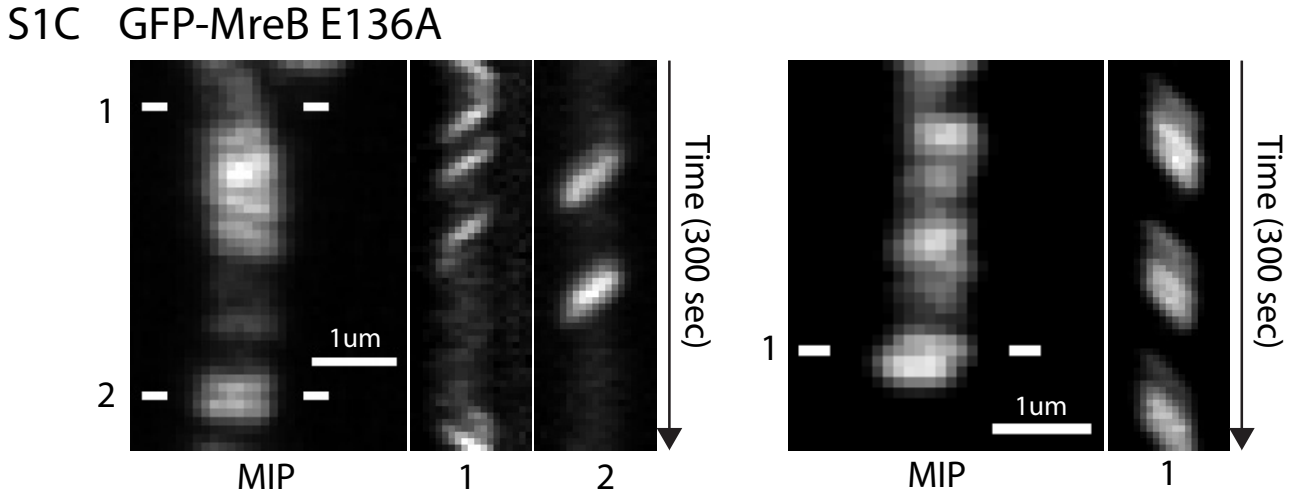

S1C – Kymographs showing axial movement in GFP-MreB (E136A) (Strain BRB770). See Supplementary Text for further discussion and movie S4 for full field movies. Maximum Intensity projection (MIP) is shown on the left.

S2A Pbp2A depletion brightfield images

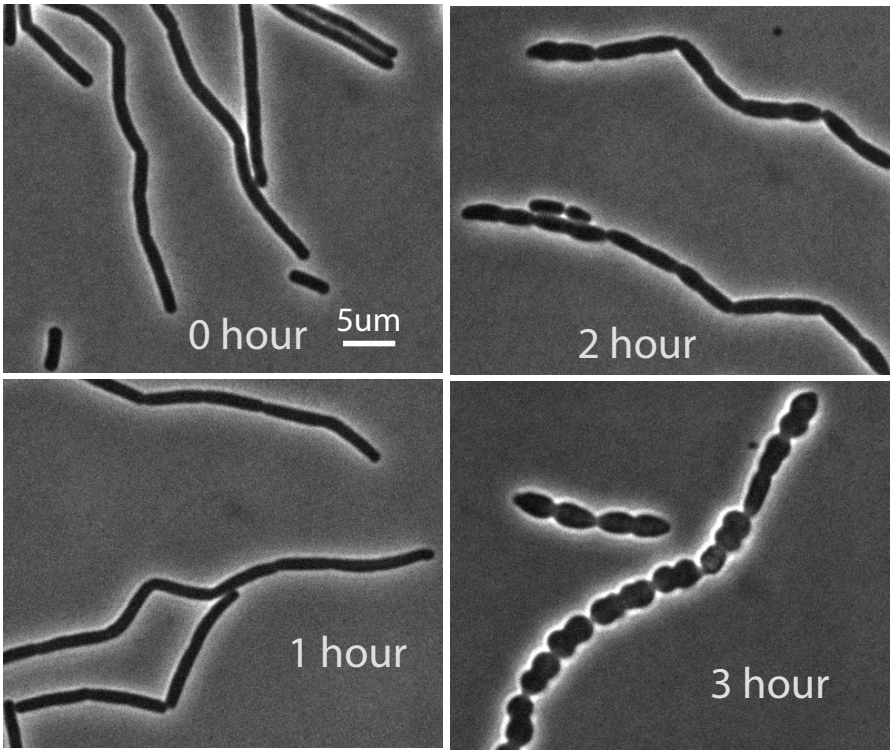

S2B RodA depletion brightfield images

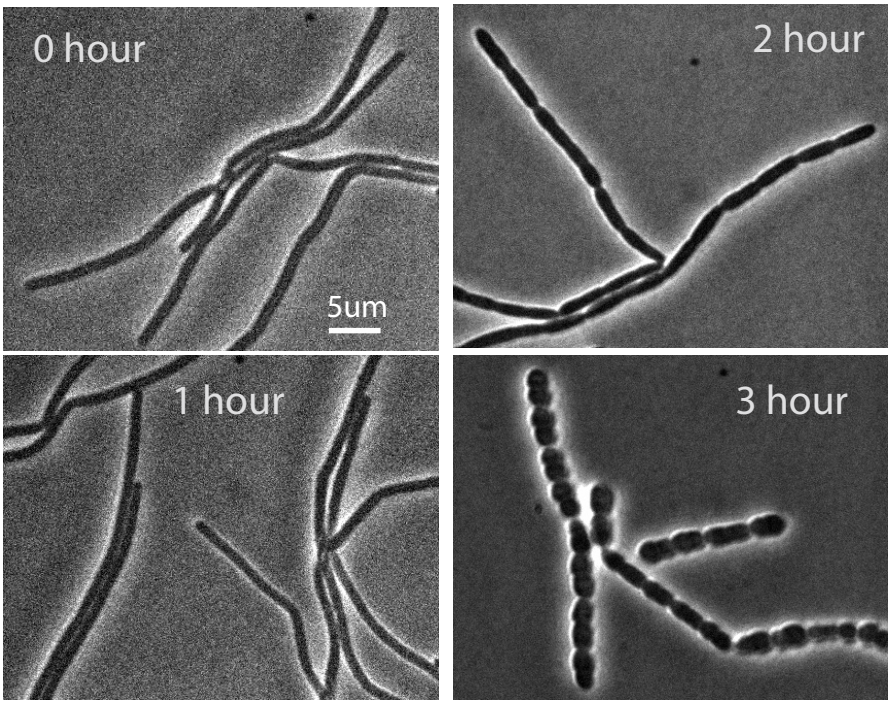

S2C RodZ depletion brightfield images

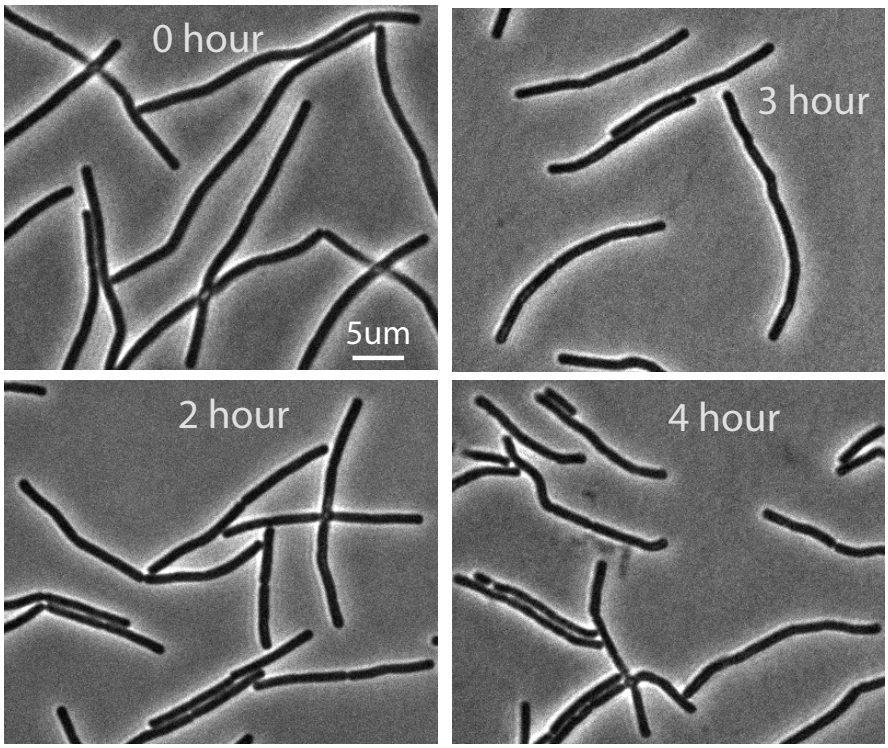

S2 – Brightfield images taken during depletion of **A)** Pbp2A (strain BRB785), **B)** RodA (strain BRB728), and **C)** RodZ (strain BRB729). Images were taken at the indicated time points after removal of IPTG and correspond to the time points of fluorescence images in Fig. 2A and movies S5A-F. Note that depletions of RodA or Pbp2A/*pbpH* lead to cell rounding, while there are only subtle morphological effects from the depletion of RodZ (YmfM) in *B. subtilis.*

S3

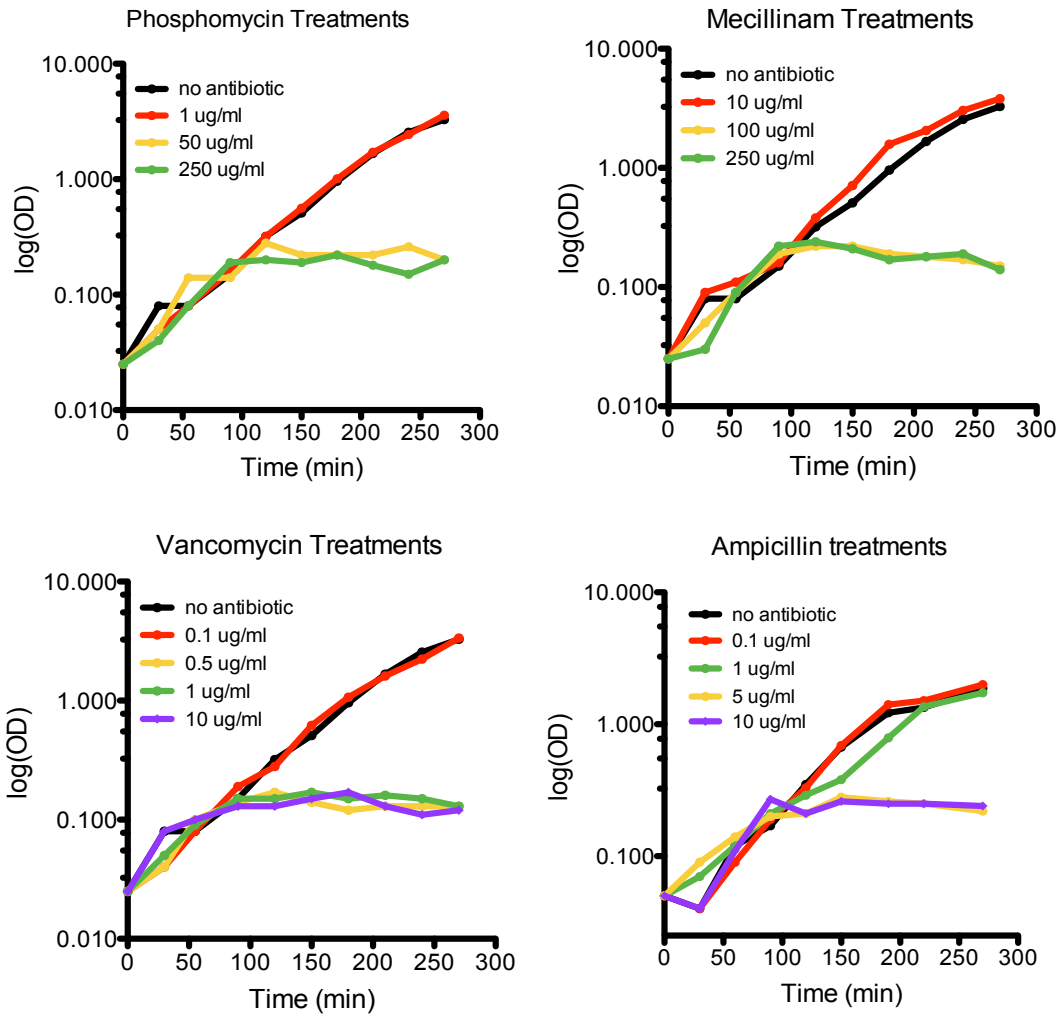

S3 – Growth curves of *B. subtilis* strain BDR2061 (37˚C, CH medium, same conditions as Fig. 2B, movies S8A-D) subjected to various antibiotic treatments. Antibiotics were added at 60 minutes, with the exception of ampicillin which was added at 75 minutes.

S4 Brightfield images of cells during foci tracking. - MreB Paralogs

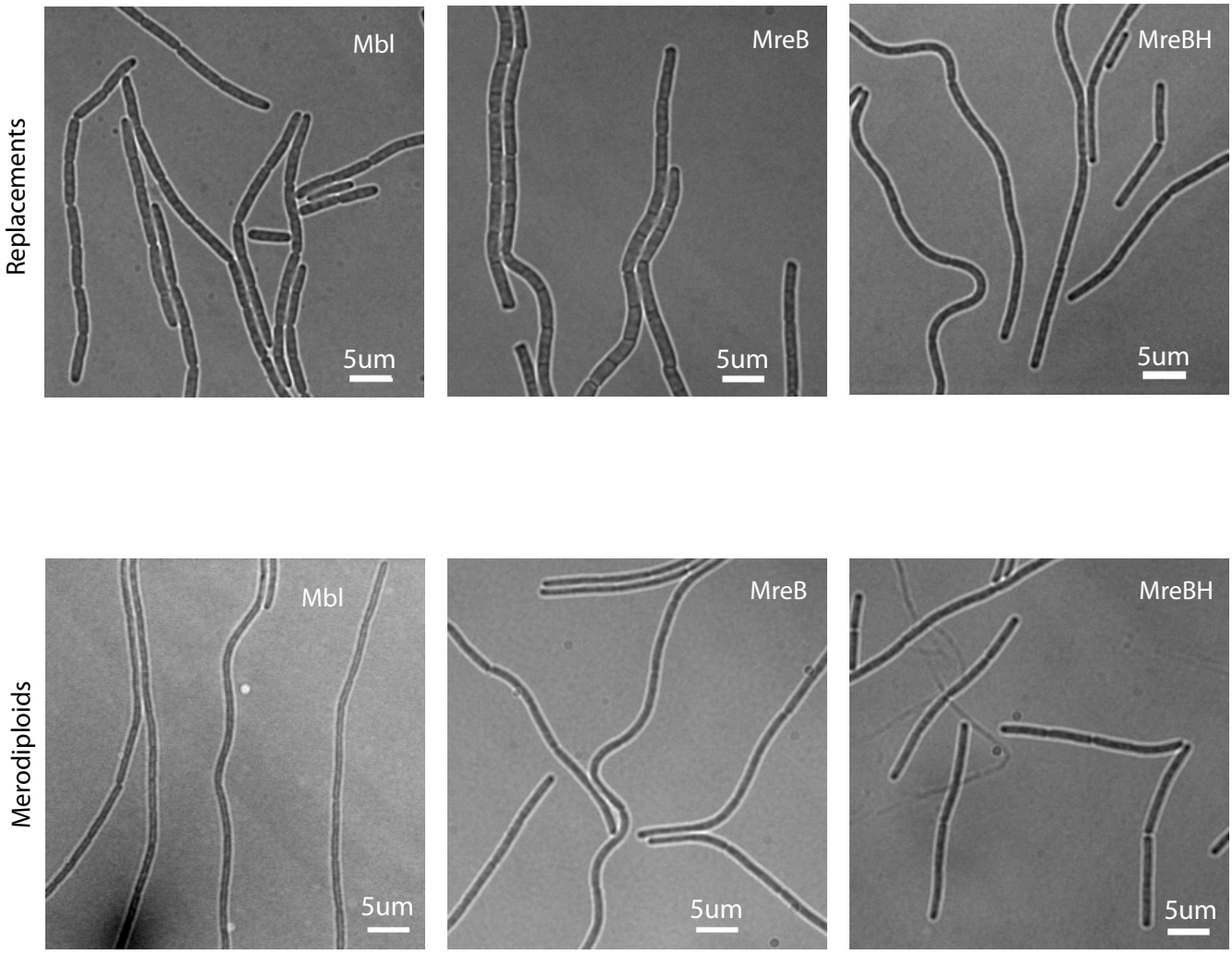

S4- Representative brightfield images of cells used to image diffraction limited foci of the MreB paralogs in both replacement and merodiploid expression conditions. Low-level expression of MreB and Mbl in replacements resulted in wider cells, which were stabilized using magnesium (*16*). MreBH replacements were also stabilized with magnesium for consistency.

S5 Brightfield images of cells during foci tracking. - PGEM proteins

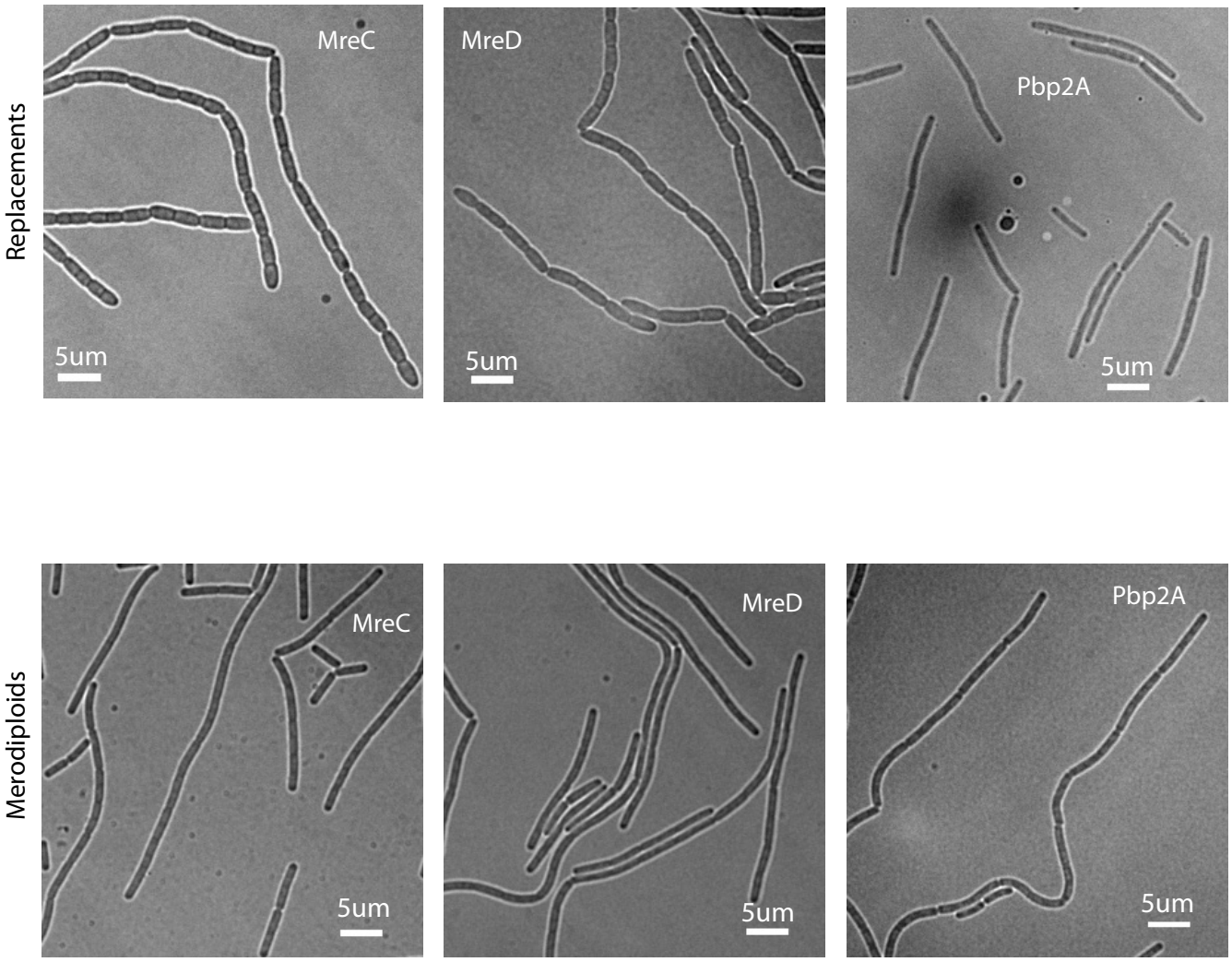

S5- Representative brightfield images of cells used to image diffraction limited foci of the PGEM proteins in both replacement and merodiploid expression conditions. Low-level expression of MreC and MreD in replacements resulted in wider cells, which were stabilized using magnesium (*16*).

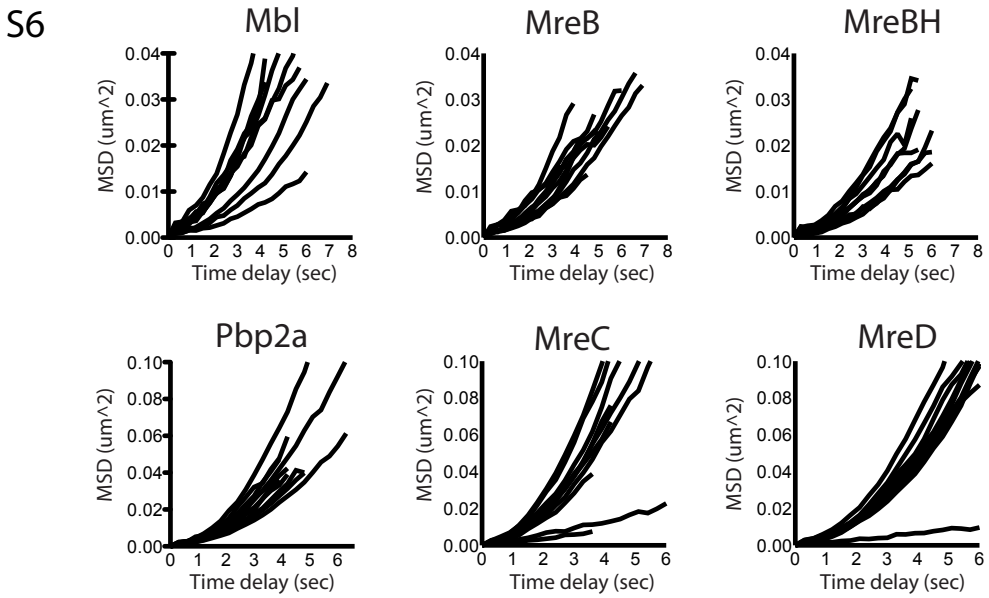

S6 – Example MSD vs. *t* traces for proteins analyzed in this study. 20 random curves for each protein are plotted from the well fit set (r^2 >0.95 fit to log(MSD) vs. log (t)). The upward curve of these traces is indicative of directed motion. Similar curves occurred for all proteins in both expression conditions.

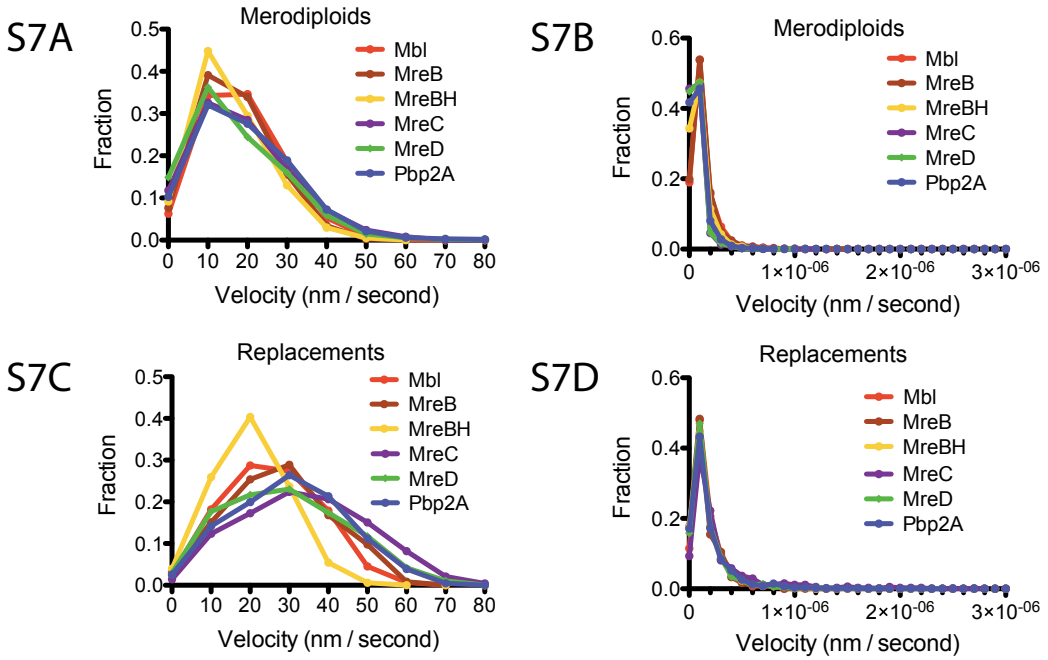

S7 – Histograms of the velocity (determined by fits to the MSD vs. *t*) for all traces (no fit criteria) above 20 frames in length **A:** All proteins expressed as merodiploids with velocity > $5x10^{-4}$ nm/sec. **B**: All proteins expressed as merodiploids with velocity ≤ $5x10^{-4}$ nm/sec. **C:** All proteins expressed as replacements with velocity > $5x10^{-4}$ nm/sec. **D**: All proteins expressed as replacements with velocity ≤ $5x10^{-4}$ nm/sec.

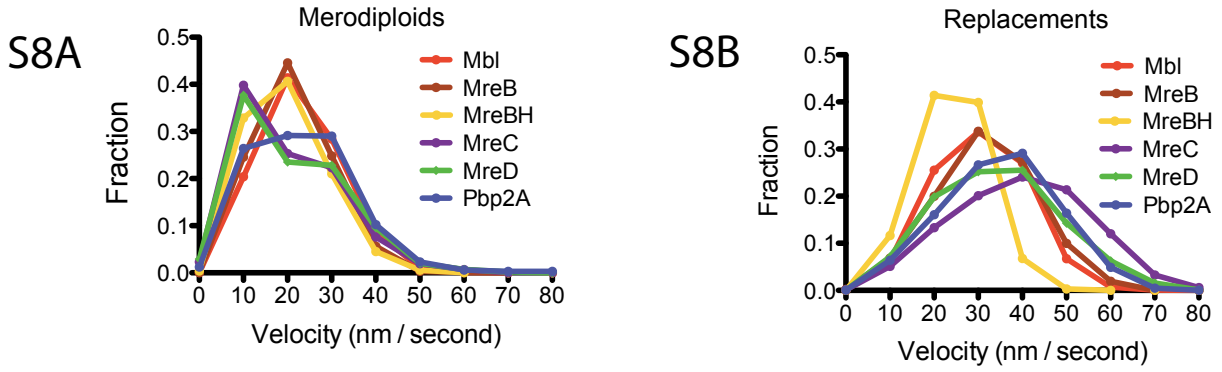

S8 - Histograms of the velocity determined using a windowed approach for traces over 20 frames in length. Velocity was determined by calculating displacement over a sliding window of 20 frames, and plotting the average value for each trace. Shown is the windowed average velocity for **A:** Proteins expressed as merodiploids (same traces as Fig. S7A) **B:** Proteins expressed as replacements (same traces as Fig. S7C).

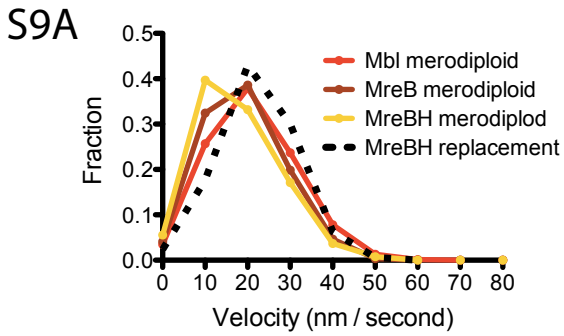

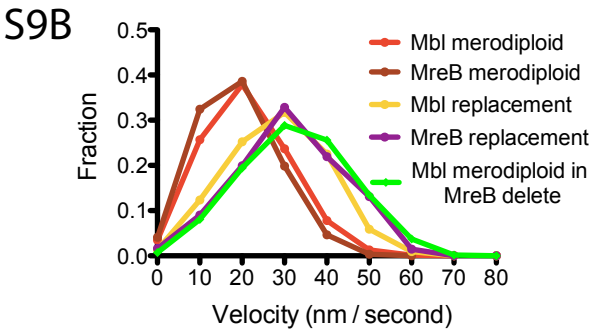

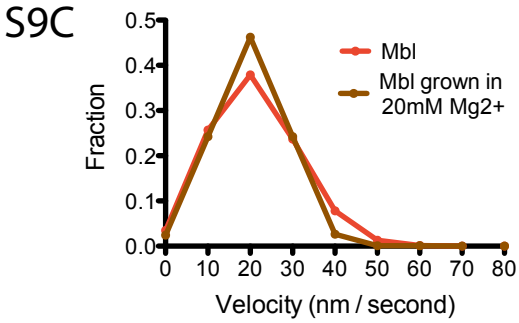

S9A –Reductions in MreBH expression as the only source (low expression as a replacement) does not cause its velocity to significantly shift. Shown in color are the velocity distributions of merodiploid expressed Mbl, MreB, and MreBH (same as in Fig. 4A). Overlayed in the dotted black line is the replacement low expression of MreBH (same as in Fig. 4B).

S9B – Increase and broadening of the velocity distributions appears to correlate with a reduction in cytoskeletal or PGEM components, even when occurring in *trans*. Shown in green is velocity distribution that arises from tracking a GFP-Mbl merodiploid strain where MreB has been deleted (original strain is the Mbl red line). For comparison the Mbl and MreB velocity distributions from both the replacements and merodiploids (from Figs. 4A and 4B) are overlayed.

S9C – Growth in 20mM $MgCl_2$ does not change the rate of GFP-Mbl motion. Shown is particle tracking of well-fit traces of GFP-Mbl expressed as a merodiploid grown in CH (same as in Fig. 4A) and when grown and imaged in CH supplemented with 20mM $MgCl_2$.

S10A

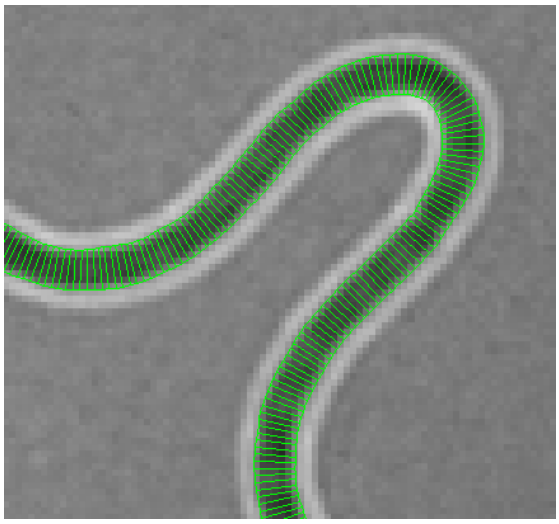

S10B

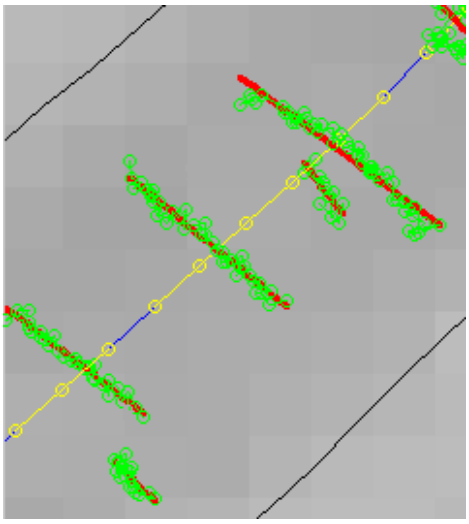

S10 – Examples demonstrating how the local midline of cells was determined by the segmentation of brightfield images. Brightfield images were acquired and MicrobeTracker (*3*) was used to gain an X-Y coordinate mesh for the outside of each chain of cells. Shown in Fig. S10A is a representative brightfield image with an overlayed mesh (green), with vectors connecting each side of the mesh. The midpoint of these vectors is used to determine a local midline. Shown in Fig. S10B is an example of the determination of angles to this midline. First, the average point of each trace was computed, and the nearest midpoint located. The traces (shown in green) were then fit by a linear fit (shown in red). The local midline was then defined by extending the nearest midpoint by 1 point on either side (shown in yellow). The angle of intersection was then computed between the trace line (red) and local midline (yellow). Due to TIRF illumination and cell curvature, foci only traverse a fraction of the cell width, so traces did not have to intersect the local midline to be considered.

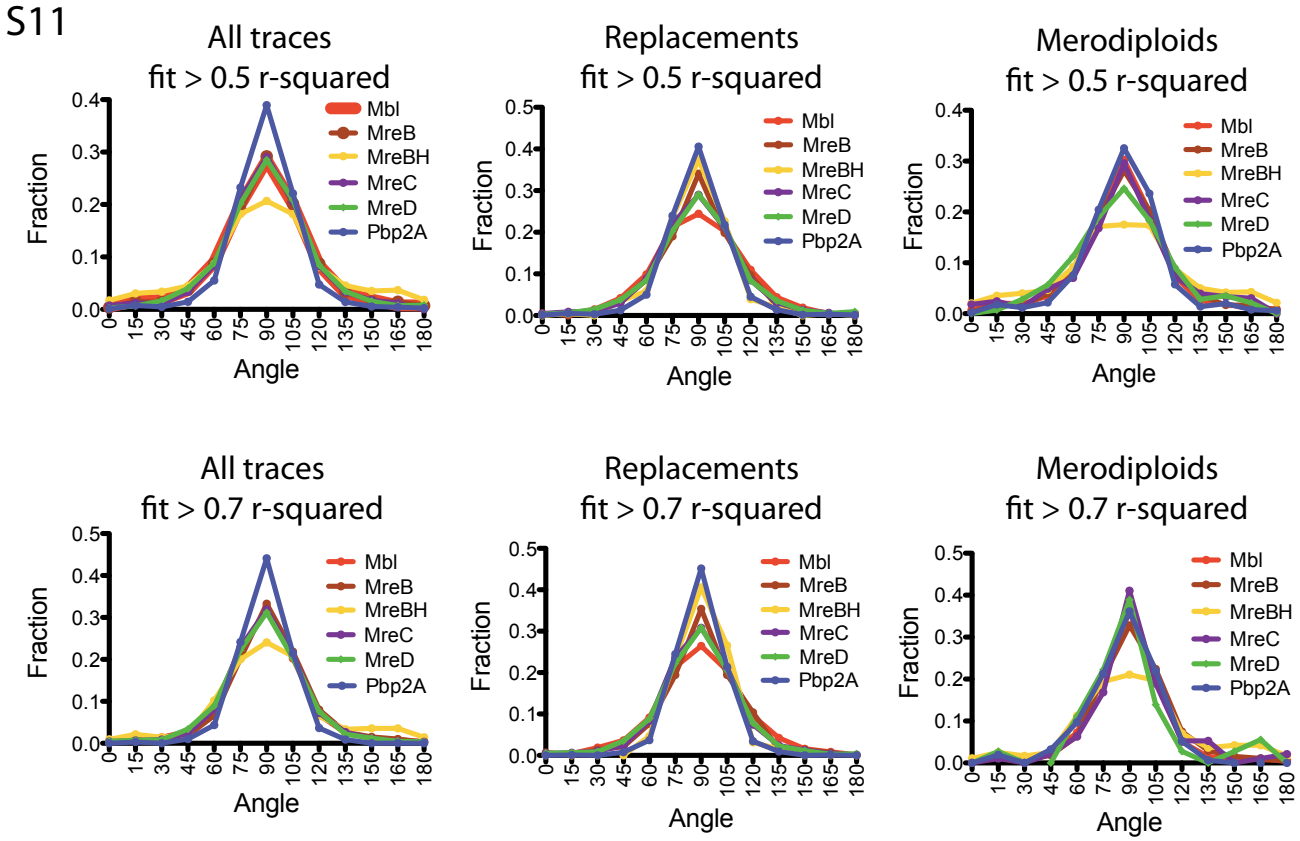

S11 - Distributions of the angles that traces intersect the midline of the cell, showing traces combined from both expression conditions (upper left is same as Fig. 4C) and also showing each expression condition independently. Shown on top are traces that could be fit with straight line with $r^2 > 0.5$. Shown on the bottom are traces that could be fit with line with $r^2 > 0.7$, demonstrating that as the stringency of fit is increased the distribution becomes more narrow (Table S2).

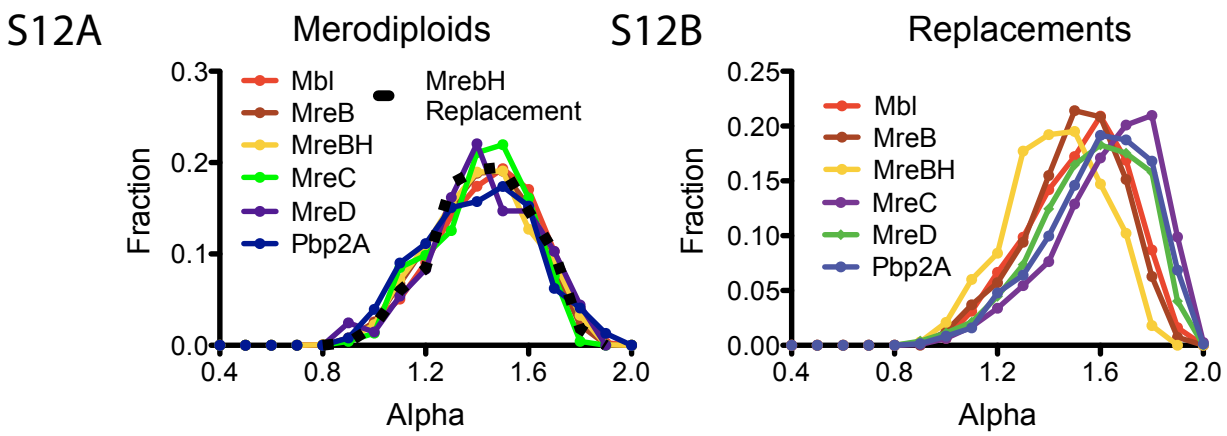

S12 – Histograms of the scaling coefficient α. α is defined as the slope of log(MSD) vs. log(t) plots (*i.e.* the log-log plot of curves as in Fig. S6) (*14*). α provides a measure of whether the motion is diffusive (α=1), subdiffusive (α<1) or directed (1<α<2). α=2 indicates motion at a constant velocity and direction, while 1 < α < 2 indicates active motion that varies in velocity or direction. Shown are well fit traces (r^2>0.95 fit to log(MSD) vs. log(t)) above 20 frames in length (as used in Figs. 4A and B) with velocity > $5x10^{-4}$ nm/sec for: **Left:** All merodiploid strains, **Right:** all replacement strains. The fact that these α distributions are centered > 1 indicates that these proteins are moving in a directed, active manner (mean value for merodiploids ~1.5, mean value for replacements ~1.4, Table S2). The MreBH-replacement is plotted on the merodiploid plot (dotted black line) to show its overlap with the merodiploid curves, similar to its overlap with the merodiploid velocity curves in Fig. S9A.

S13

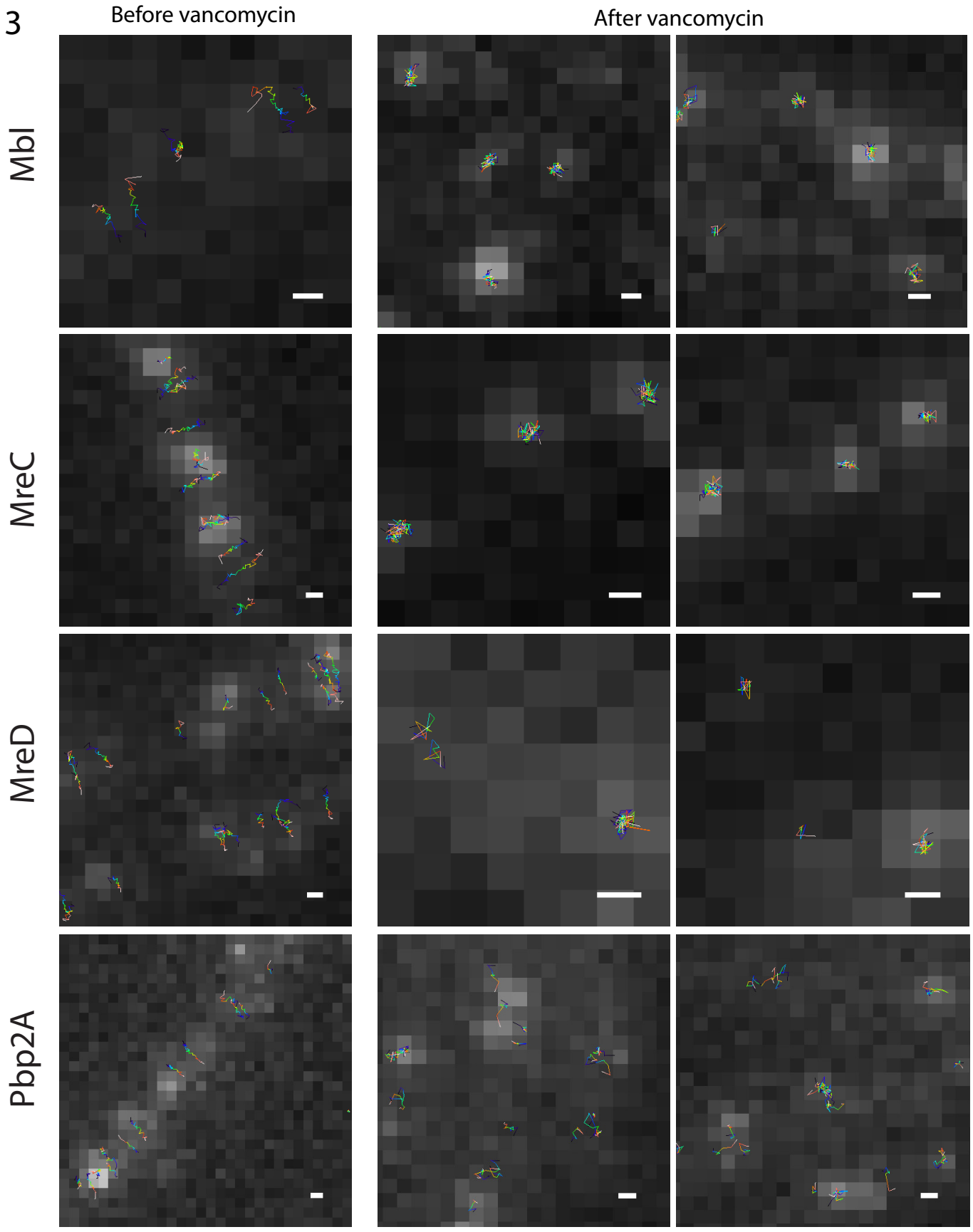

S13– Treatment with vancomycin abolishes the axial movements of Mbl (expressed as a merodiploid), and MreC, MreD, and Pbp2A (expressed as replacements). Shown are raw tracking data where the same slide has been imaged before (left) and after (right) the addition of 2µl of 5mg/ml vancomycin to a 1.5mm thick agar pad (600µl total volume). While vancomycin stops the directed, circumferential motions of all proteins shown, the treatments resulted in completely immobile foci for Mbl and mostly immobile foci for MreC and MreD. This is manifest as the foci stay confined in a small area (under one pixel) for the entire imaging period (100 seconds) (please note scale change between panels). Pbp2A foci displayed a different behavior, where a few foci became static, but the majority of foci became apparently diffusive on the membrane, moving in random directions of which our small (117nm) tracking radius could only capture a small fraction of their trajectory. Slides were imaged 2-5 minutes after the addition of vancomycin. Scale bars are 200nm. See movie S12A for a movie of foci after treatment.

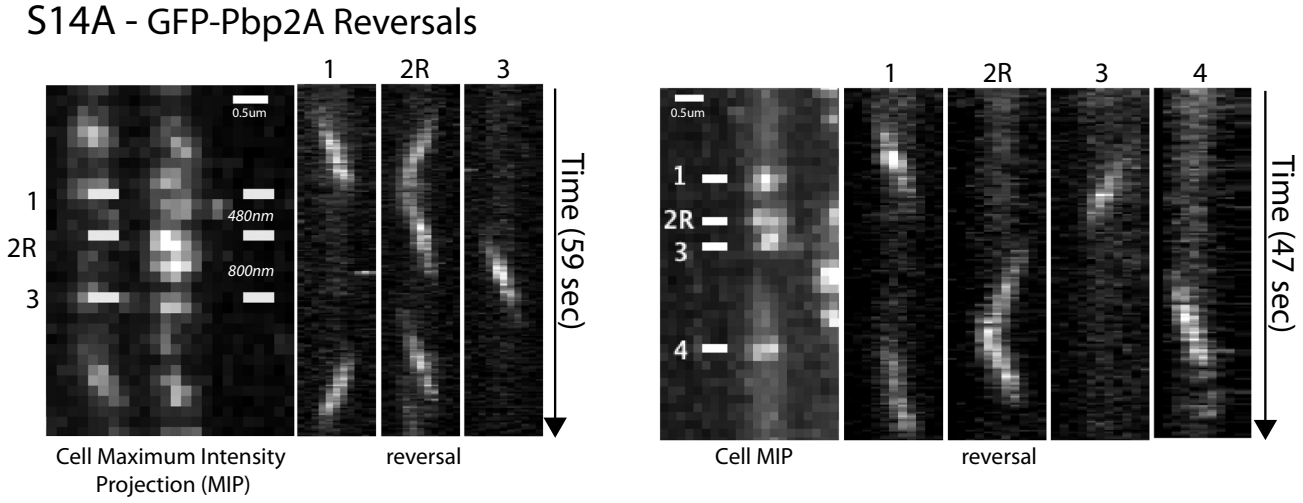

S14A – Kymographs of single particle TIRF movies for GFP-Pbp2A (expressed as a replacement) demonstrating reversals in motion (corresponding movie S12C). Particles 1 and 3 in the left panel and particles 1, 3, and 4 in the right panel appear on one side of the cell, travel across the cell width, and disappear at the other side. When they leave the illumination plane. However, in both movies the particles indicated as "2R" travel across the cell, then reverse their direction. Note the intensity and spot width does not change before and after reversal, indicating it is within the same plane before and after reversal.

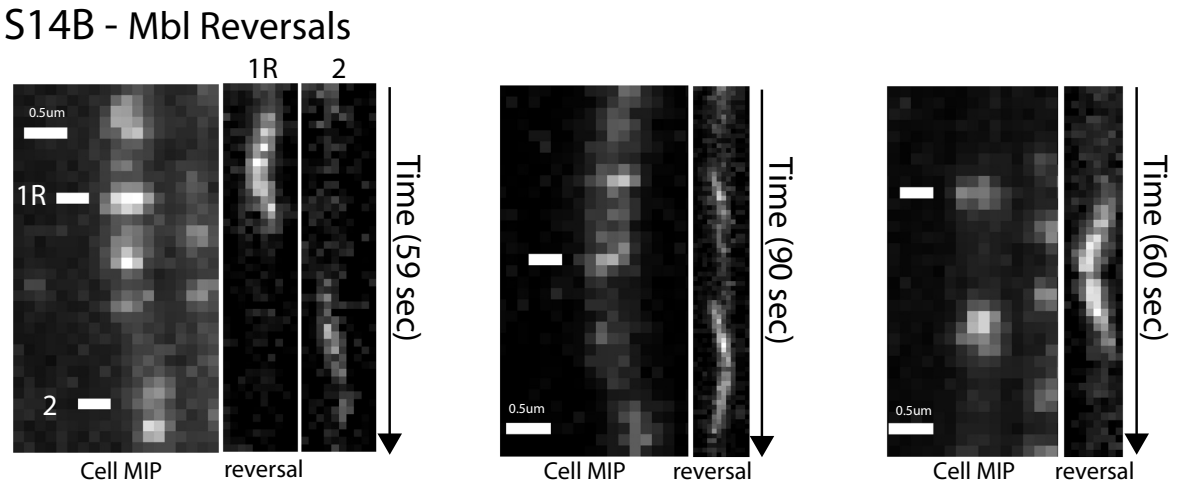

S14B – Kymographs of single particle TIRF movies for GFP-Mbl (expressed as a merodiploid) showing reversals in motion.

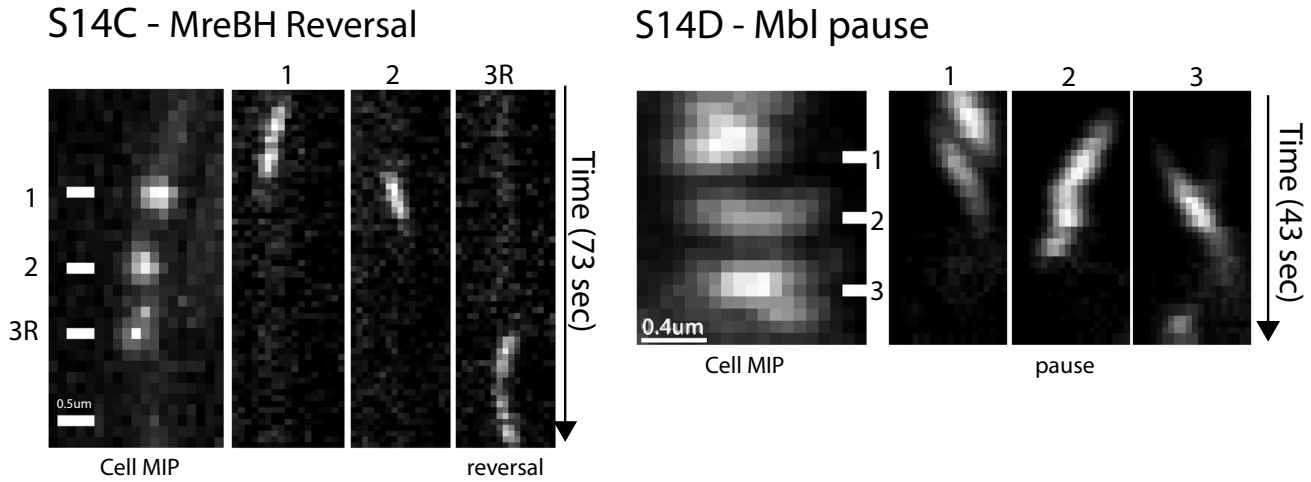

S14C – Kymographs of a single particle TIRF movie for GFP-MreBH (expressed as a replacement) demonstrating a reversal in motion.

S14D– Kymograph showing a pause in the directed motion of GFP-Mbl (expressed at high levels). Strain BDR2061 was grown in the presence of 10mM xylose, and imaged by TIRF microscopy with streaming 1-second acquisition intervals. The particle indicated at position 2 moves directionally, pauses for 7 seconds, and then resumes directional motion. Maximum Intensity projection (MIP) is shown on the left. Corresponding movie S12D.

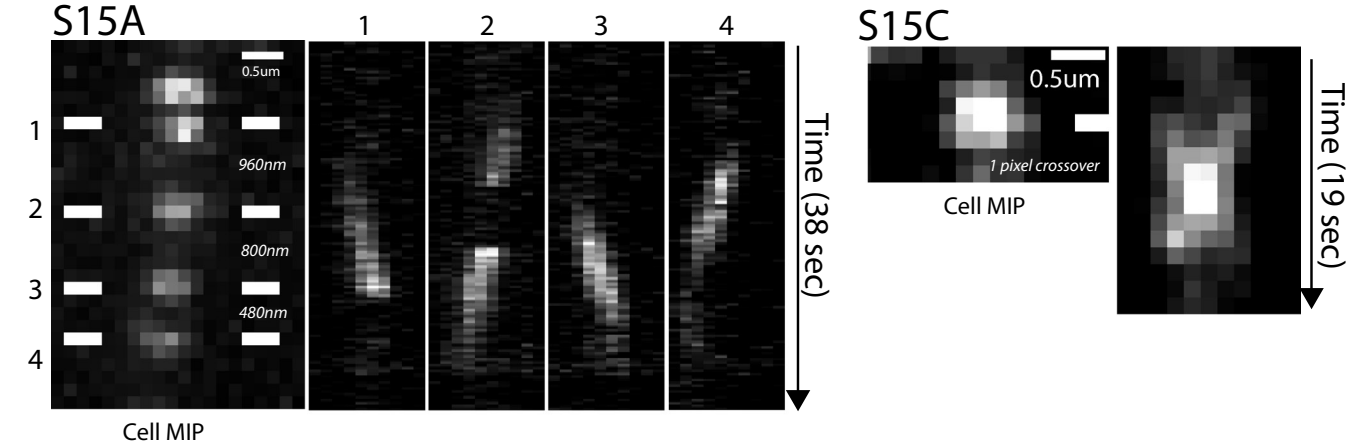

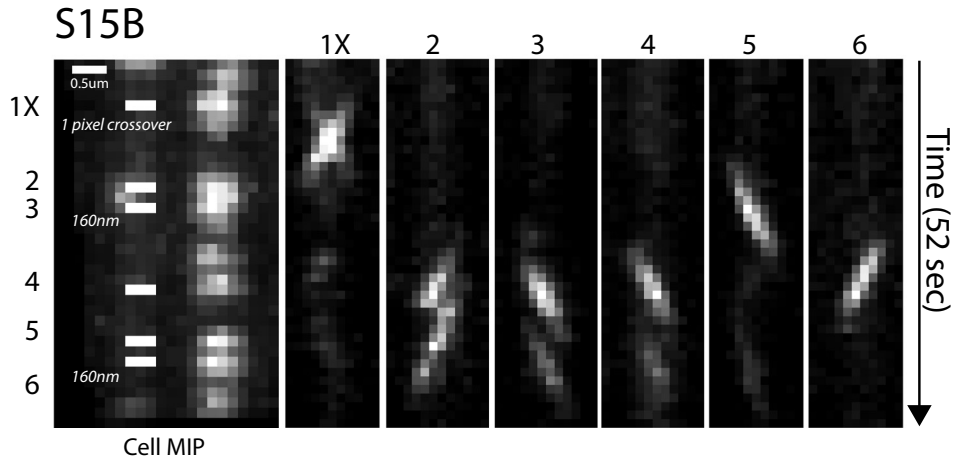

S15A - Kymographs of single particle TIRF movies for GFP-Mbl (expressed as merodiploid), showing that proximal foci on one surface of the cell move in opposing directions. Corresponding movie S13A (top movie). Particles appear on one side of the cell, travel across the cell width ~3 pixels (~480nm), and disappear at the other side (particles 2, 3, and 4) or bleach (particle 1). In this example, particles within short distances (indicated between kymograph bars) move in alternating opposite directions. Under our growth conditions, *B. subtilis* cells (within chains) are on average 3µm long. These data demonstrate that Mbl can move in opposite directions on the surface of one bacterium, as at least 2 of these traces must exist in one cell. Note that the GFP-Mbl focus indicated 2 undergoes a blinking event mid-trajectory. Each pixel is 160nm.

S15B – Similar to Fig. S15A, showing kymographs of single foci TIRF movie for GFP-Mbl moving in opposing directions. Corresponding movie S13D. Kymograph 1X displays 2 foci moving in opposing directions within a 1 horizontal pixel range, as manifested by the crossover "X" in the kymograph. Kymographs 2+3 and 5+6 show 2 particles moving in opposing directions separated by 1 pixel (160nm). Pixels are 160nm.

S15C – Kymograph showing 2 foci of GFP-Pbp2A moving in opposing directions within a 1 horizontal pixel range, as manifested by the crossover "X" in the kymograph. Corresponding movie S13C (*left*).

S16

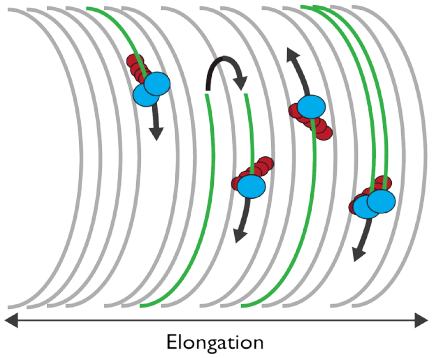

S17

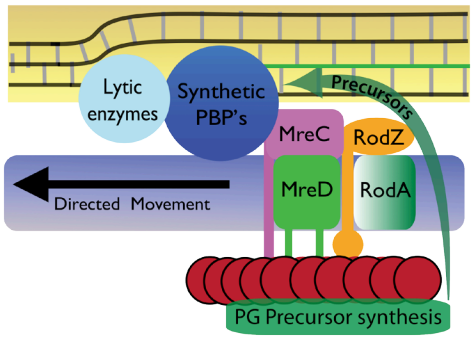

S16 - Model for the rotary insertion of new cell wall material in *B. subtilis*. PG synthetic complexes (*blue)*, which may exist as multiple or single units, and their associated MreB filaments (*red*) move axially around the cell circumference in both directions, inserting bands of new PG during their transit (*green*). These complexes can reverse their motion, which may reflect the cessation of one synthetic event and the initiation of a new radial band.

S17 - Model for the directed motions of the PG elongation machinery and MreB filaments. PG precursor generating enzymes, bound to MreB, provide a local pool of lipid-linked muropeptide precursors (*green arrow*) that PBPs incorporate into the newly synthesized glycan strands (*green*). Their processive insertion drives the movement of the PG elongation machinery along the cell wall, pulling the associated MreB filaments and precursor synthesis complexes.

Supplemental Movie Legends
Movies are available at http://mitchison.med.harvard.edu/cellwall/
Note from the authors: Due to the short duration of these movies, we suggest you loop them during playback.

S1A- Timelapse stack of strain BDR2061 where GFP-Mbl is expressed under the control of a xylose-inducible promoter as the sole source of Mbl in the cell. GFP-Mbl expression was induced using 10mM xylose. Frames are 5 seconds apart.

S1B- Movie of kymograph analysis in Fig. 1A. Lines used for kymograph analysis are drawn between white bars. Frames are 5 seconds apart.

S2A- Timelapse stacks showing the axial movement of the three MreB paralogs in merodiploid strains. Shown are BDR2437 (GFP-Mbl) BDR2436 (GFP-MreB), and BDR2438 (GFP-MreBH.) All three GFP-fusions are under xylose control and are expressed in the presence of wild-type copies of the proteins. Expression of all three GFP fusions was induced with 10mM xylose. Frames are 5 seconds apart.

S2B- Movie of kymograph analysis in Fig. 1B, showing strains BDR2437 (GFP-Mbl), BDR2436 (GFP-MreB), BDR2438 (GFP-MreBH), and a hydrolysis deficient GFP-MreB BRB736 (GFP-MreB-D158A) (*far right*). Frames are 5 seconds apart.

S3A- Kymograph analysis of EpsE-GFP (strain BDR2450) in Fig. 1C. Frames are 10 seconds apart.

S3B- Two-color spinning disk confocal imaging of strain BRB783 (EpsE-GFP, PxylA-mCherry-MreB). The EpsE-GFP signal is false-colored red, mCherry-MreB is false-colored green. Expression of mCherry-MreB was induced with 10mM xylose. Frames are 10 seconds apart.

S4- Timelapse stacks demonstrating that GFP-MreB mutants impaired in ATP hydrolysis still undergo axial motion. First shown is strain BRB736, where GFP-MreB (D158A) (*7*) is expressed as a merodiploid under xylose control. Next shown is BRB770, which expresses GFP-MreB containing the E136A mutation, an equivalent mutation to one that completely blocks ATP hydrolysis in ParM (*9*), and postulated to do so in eukaryotic actin (*8*). Both strains were induced with 10mM xylose and imaged after 1 hour. Frames are 5 seconds apart. The next two image sequences examine the effects of expressing an unlabeled hydrolysis-deficient MreB (D158A) on the dynamics of wild-type GFP-MreB. This strain (BRB755) expresses GFP-MreB under xylose control, and also contains an IPTG-inducible unlabeled MreB(D158A). This strain was grown in the presence of 10mM xylose to an OD600 of 0.5 to express GFP-MreB, and imaged prior to the addition of IPTG (indicated by time 0). Cells were then diluted into fresh media with 10mM xylose and 1mM IPTG, and imaged after 1 hour. While the expression of MreB(D158A) changed the localization of GFP-MreB, axial motion was still apparent in areas that were not obscured by complete transverse bands. Example positions that exhibit axial motion are indicated by white bars undeneath. Frames are 5 seconds apart. Further discussion of these mutants and comparisons with previous studies are provided in Supplementary Text.

S5A- Kymograph analysis of GFP-Mbl during RodA depletion from strain BRB728 as in Fig. 2A. Frames are 5 seconds apart. Partial freezing is observed at 2 hours.

S5B- Overview of GFP-Mbl dynamics during RodA depletion from strain BRB728, showing that round cells display impaired GFP-Mbl dynamics, while more rod-like cells still display normal dynamics. Movie was taken 2.5 hours after the removal of IPTG. Frames are 5 seconds apart.

S5C- Kymograph analysis of GFP-Mbl during Pbp2A depletion in a strain lacking PbpH (BRB785) as in Fig. 2A. Frames are 5 seconds apart. Partial freezing is observed at 2 hours.

S5D- A collection of cells at indicated time points from strain BRB785 (imaging GFP-Mbl as in movie S5C) during Pbp2A depletion. Frames are 5 seconds apart. Partial freezing is observed at 2 hours.

S5E- Kymograph analysis of GFP-Mbl during RodZ depletion (strain BRB729) as in Fig. 2A. Frames are 5 seconds apart. Partial freezing is observed at 3 hours.

S5F- A collection of cells at indicated time points from strain BRB729 (imaging GFP-Mbl as in movie S5E) during RodZ depletions. Frames are 5 seconds apart. Partial freezing is observed at 3 hours.

S6A- Overview of BDR2061 treated with cell wall inhibiting antibiotics, using thick pads and low concentrations to provide a contrast between the period of motion and the period of freezing. Drugs were added to the top of 1.5mm thick agar pads immediately before or within 30 seconds of the start of imaging. Frames are 10 seconds apart. GFP-Mbl was induced with 10mM xylose.

S6B- Kymograph analysis of BDR2061 treated with cell wall inhibiting antibiotics as in Fig. 2B and movie S6A. Frames are 10 seconds apart.

S6C- Demonstration of the rapidity of GFP-Mbl freezing following the addition of cell wall inhibiting antibiotics to cells under thin agar pads. Strain 2061 (grown in the presence of 10mM xylose) was placed on a coverslip, and covered with a very thin agar pad. Image acquisition was started, and antibiotics were then added to the top of the pads between frame 20 and 21. Frames are 10 seconds apart. Cessation of axial motion occurred within 1 frame with the addition of 50μg/ml vancomycin, within 3 frames for 5μg/ml vancomycin, and within 2-3 frames with 10μg/ml ampicillin.

S6D- Examples of freezing of GFP-MreB and GFP-MreBH when treated with cell wall inhibiting antibiotics. Shown are BDR2436 (GFP-MreB) and BDR2438 (GFP-MreBH) expressed with 10mM xylose. Mecillinam was added to the top of 1.5mm thick agar pads 30 seconds after the start of imaging. Frames are 10 seconds apart. Similar freezing is observed with these strains using vancomycin, ampicillin, and phosphomycin (Data not shown).

S7A- Overview of strain BDR2061 (GFP-Mbl) treated with antibiotics that do not target cell wall synthesis. Shown are cells that were subjected to 2-minute pretreatments (as in movies S8A-D) with high concentrations of the indicated non-cell wall targeting drugs. Treatments to the top of agar pads (as in S6A) also had no effect on filament motion even at high concentrations (Data not shown). Frames are 10 seconds apart.

S7B- Kymograph analysis of strain BDR2061 (GFP-Mbl) treated with antibiotics that do not target cell wall synthesis as in Fig. 2C and movie S7A. Frames are 10 sec apart.

S8(A-D)– Movies of strain BDR2061 (GFP-Mbl) showing the dose effects of vancomycin (movie S8A), ampicillin (movie S8B), phosphomycin (movie S8C), and mecillinam (movie S8D) on GFP-Mbl motion. Cells from exponential phase cultures were incubated for 2 minutes (with shaking) with the indicated final concentration of antibiotics, spotted onto a coverslip, covered with an agar pad, and immediately imaged. Total time between the end of incubation and imaging was 1-2 minutes. Frames are 5 seconds apart.

S9A- Montage of movies showing examples of particle tracking. Shown are diffraction-limited foci expression conditions of GFP-Mbl (BDR2437, merodiploid), GFP-MreC (BDR2448, replacement), and GFP-Pbp2A (BDR2444 replacement). Tracked particles are identified by yellow box. Traces are colored in blue to red from their beginning to end. For reference, a pixel is 160nm. Frames are 300 msec apart. Movie is 100x real time. Only foci that are identified as Gaussians and followed over 8 frames are indicated by yellow boxes and traces.

S9B- Sample of raw TIRF data of single foci of merodiploid expressed GFP-Mbl (BDR2437). Frames are 300 msec apart. Movie is 200x real time. For reference, a pixel is 160nm.

S9C- Sample of raw TIRF data of single foci of GFP-MreB (BRB795) expressed at low levels as a replacement. Frames are 300 msec apart. Movie is 200x real time. For reference, a pixel is 160nm.

S10A- Samples of raw data of single foci of GFP-MreC (BDR2448) expressed at low levels as a replacement. Frames are 300 msec apart. For reference, a pixel is 160nm. Frames are 300 msec apart. Movie is 200x real time.

S10B- Samples of raw data of single foci of GFP-MreD (BDR2447) expressed at low levels as a replacement. For reference, a pixel is 160nm. Frames are 300 msec apart. Movie is 200x real time.

S10C- Samples of raw data of single foci of GFP-Pbp2A (BDR2444) expressed at low levels as a replacement. For reference, a pixel is 160nm. Frames are 300 msec apart. Movie is 200x real time.

S11- Montage showing samples of raw TIRF data of merodiploid expressed GFP-MreC (BDR690), GFP-MreD (BDR692), and GFP-Pbp2A (BRB684). While many PGEM foci expressed via this method this rapidly diffuse across the membrane, directional movements are also observed. Examples of foci that move directionally are marked by white lines beneath their positions. Note that the fast diffusing population interferes with the tracking of the slow directionally moving foci, making tracking of merodiploids PGEM foci difficult. Frames are 300 msec apart. Movie is 200x real time. For reference, a pixel is 160nm.

S12A- Movies of foci of GFP-Mbl (merodiploid), GFP-MreB (replacement), GFP-MreC (replacement), and GFP-MreD (replacement) 2-5 minutes after vancomycin has been added to the pad as in Fig. S13 (2µl of 5mg/ml vancomycin to a 1.5mm thick agar pad, 600µl total volume). Frames are 300 msec apart. Movie is 100x real time. Pixels are 160nm.

S12B- Montage of GFP-Pbp2A foci undergoing transitions from moving to immobile states (pauses) taken from TIRF particle tracking data. Positions of foci that pause are indicated by arrows. For reference, a pixel is 160nm. Frames are 300 msec apart. Movie is 200x real time.

S12C- Movies (as in Fig. S14A) of GFP-Pbp2A particles undergoing reversals in motion, while adjacent particles go in and out of the illumination plane as they cross the cell width. For reference, a pixel is 160nm. Frames are 300 msec apart. Movie is 200x real time.

S12D- Movie of a pause observed in GFP-Mbl motion seen in strain BDR2061 (as in Fig. S14D). Strain BDR2061 was induced with 10mM xylose, and imaged via TIRF microscopy with streaming 1-second acquisition intervals. The particle indicated at position 2 moves directionally, pauses for 7 seconds, and then resumes directional motion. Frames are 1 second apart.

S13A- Movies (as in Fig. 4E (*bottom movie*) and Fig. S15A (*top movie*)) of proximal GFP-Mbl (BDR2437) foci moving in opposing directions across the cell surface taken from particle tracking movies. Frames are 300 msec apart. Movie is 200x real time. Pixels are 160nm.

S13B- TIRF imaging of highly expressed GFP-Mbl in strain BDR2061, showing that proximal movements occur in both directions across the cell surface, even when MreB paralogs are expressed at high levels. Strain BDR2061 was induced with 10mM xylose, and imaged via TIRF microscopy with streaming 1-second acquisition intervals. Frames are 1 second apart.

S13C- Movies (as in Fig. 4F (*right movie*) and S15C (*left movie*)) of extremely proximal GFP-Pbp2A (BDR2444) foci moving in opposing directions on one surface. Frames are 300 msec apart. Pixels are 160nm.

S13D- Movie (as in Fig. S15B) of extremely proximal GFP-Mbl (BDR2437) foci moving in opposing directions on one surface. Kymograph 1X displays 2 foci moving in opposing directions within a 1 horizontal pixel range, and 2+3 and 5+6 show 2 sets of particles moving in opposing directions separated by 1 pixel (160nm). Frames are 300 msec apart. Pixels are 160nm.

Supplemental Tables

Supplemental Table S1 – Mean inhibitory concentration (MIC) of cell-wall inhibiting antibiotics

Measured in strain 2061, CH, 10mM xylose, 37°C. See also Fig. S3.

Antibiotic	**MIC**
Vancomycin	0.5μg/ml
Ampicillin	5μg/ml
Phosphomycin	50μg/ml
Mecillinam	100μg/ml

Supplemental Table S2 – Particle tracking statistics.
Rows in bold indicate data used in Figs. 4, S8, S9, and S12.

All traces used are over 20 frames in length
"**MFit**" indicates r^2 cutoff of linear fit to log (MSD) vs. log (*t*).
"Rfit" indicates r^2 cutoff of linear fit to trace.
"**Low velocity**" indicates MSD vs. *t* derived velocity ≤$5x10^{-4}$ nm/second.
"**High velocity"** indicates MSD vs. *t* derived velocity > $5x10^{-4}$ nm/second.

Number of traces – Replacements (all traces over 20 frames in length).						
	Mbl	**MreB**	**MreBH**	**MreC**	**MreD**	**Pbp2A**
Total traces	4320	1521	1110	2805	3092	4694
# High velocity (% of total traces)	3054 (70.6%)	921 (60.5%)	679 (61.2%)	2013 (71.8%)	1968 (63.6%)	3485 (74.2%)
# Low velocity (% of total traces)	1266 (29.3%)	600 (39.5%)	431 (38.8%)	792 (28.2%)	1124 (36.4%)	1209 (25.8%)
# Traces Mfit > 0.95 (% of total traces)	2150 (49.8%)	567 (37.3%)	359 (32.3%)	1685 (60.7%)	1376 (44.5%)	2733 (58.2%)
# High velocity Mfit > 0.95 (% of #MFit > 0.95)	**2056 (95.6%)**	**542 (95.6%)**	**333 (92.8%)**	**1598 (94.8%)**	**1318 (95.8%)**	**2637 (96.5%)**
# Low velocity Mfit > 0.95 (% of #MFit > 0.95)	94 (4.4%)	25 (4.4%)	26 (7.2%)	87 (5.2%)	58 (4.2%)	96 (3.5%)

Number of traces – Merodiploids (all traces over 20 frames in length).						
	Mbl	**MreB**	**MreBH**	**MreC**	**MreD**	**Pbp2A**
Total traces	15252	9230	5882	4082	2582	8380
# High velocity (% of total traces)	8757 (57.4%)	5112 (55.4%)	3190 (54.2%)	1130 (27.7%)	544 (21.1%)	2037 (24.3%)
# Low velocity (% of total traces)	6495 (42.6%)	4118 (44.6%)	2692 (45.8%)	2952 (72.3%)	2038 (78.9%)	6343 (75.7%)
# Traces Mfit > 0.95 (% of total traces)	5066 (33.2%)	2853 (30.9%)	1866 (31.7%)	247 (6.1 %)	148 (5.7%)	684 (8.2%)
# High velocity Mfit > 0.95 (% of #MFit > 0.95)	**4649 (91.8%)**	**2575 (90.3%)**	**1676 (89.8%)**	**223 (90.3%)**	**137 (92.3%)**	**610 (89.2%)**
# Low velocity Mfit > 0.95 (% of #MFit > 0.95)	417 (8.2%)	278 (9.7%)	190 (10.2%)	24 (9.7%)	11 (7.7%)	74 (10.8%)

Mean Velocity – Replacements (all values in nm / second)						
Reported as: Mean, *StdDev*	**Mbl**	**MreB**	**MreBH**	**MreC**	**MreD**	**Pbp2A**
MSD Velocity – No fit All traces, High velocity	25.6,*11.7*	29.9,*13.6*	20.1, *9.2*	34.1, *16.0*	29.3, *15.3*	30.1, *14.1*
MSD Velocity – No fit All traces, Low velocity	1.9E-7 2.3E-7	1.7E-7 1.8E-7	1.6E-7 *1.5E-8*	2.8E-7 *3.6E-7*	1.7E-7 *1.9E-7*	1.9E-7 *2.3E-7*
MSD Velocity, High velocity, Mfit > 0.95	**28.2, *11.4***	**30.8,*12.1***	**22.0,*8.6***	**37.5, *15.0***	**33.9, *14.8***	**33.4, *13.2***
MSD Velocity Low velocity, Mfit > 0.95	4.0E-7 *2.5E-7*	4.4E-7 *3.1E-7*	3.3E-7 *1.4E-7*	7.5E-7 *5.5E-7*	4.6E-7 *3.5E-7*	5.6E-7 *4.3E-7*
Windowed velocity All traces, high velocity	**26.6, *11.3***	**25.8,*12.7***	**20.9, *8.6***	**34.3, *16.3***	**28.1, *15.0***	**30.4, *14.1***

Mean Velocity – Merodiploids (all values in nm / second)						
Reported as: Mean, *StdDev*	**Mbl**	**MreB**	**MreBH**	**MreC**	**MreD**	**Pbp2A**
MSD Velocity – No fit All traces, High velocity	18.54, *9.9*	16.9,*9.2*	15.7, *9.1*	18.7,*12.4*	17.5,*12.7*	20.0,*14.9*
MSD Velocity – No fit All traces, Low velocity	1.3E-7 1.3E-7	1.3E-7 1.3E-7	1.0E-8 *9.8E-8*	7.4E-8 *8.2E-8*	7.4E-8 *9.1E-8*	8.8E-8 *8.6E-8*
MSD Velocity, High velocity, Mfit > 0.95	**21.2, *9.9***	**18.9, *9.1***	**17.6, *9.3***	**26.3,*12.3***	**27.9,*13.9***	**27.8, *18.9***
MSD Velocity Low velocity, Mfit > 0.95	3.5E-7 *2.3e-7*	3.5E-7 *2.4E-7*	2.4E-7 *1.8E-7*	4.3E-7 *2.4E-7*	6.3E-7 *7.4E-7*	3.4E-7 *1.9E-7*
Windowed velocity All traces, high velocity	**19.2, *8.9***	**18.0, *8.2***	**16.4, *8.3***	**20.0, *11.2***	**20.9, *13.0***	**23.6, *13.0***

Mean Alpha – Replacements						
Reported as: **Mean, *StdDev***	**Mbl**	**MreB**	**MreBH**	**MreC**	**MreD**	**Pbp2A**
MSD alpha All traces, High velocity	1.38, *0.29*	1.23, *0.30*	1.24, *0.28*	1.51, *0.31*	1.39, *0.34*	1.46, *0.31*
MSD alpha Low velocity, All traces	0.49, *0.46*	0.32, *0.50*	0.41, *0.47*	0.54, *0.51*	0.37, *0.47*	0.42, *0.50*
MSD alpha **High velocity, Mfit > 0.95**	**1.51, *0.19***	**1.50, *0.19***	**1.42, *0.18***	**1.62, *0.20***	**1.56, *0.20***	**1.59, *0.20***
MSD alpha Low velocity, Mfit > 0.95	1.09, *0.12*	1.04, *0.14*	1.07, *0.13*	1.21, *0.19*	1.03, *0.19*	1.09, *0.20*
Mean Alpha - Merodiploids						
Reported as: **Mean, *StdDev***	**Mbl**	**MreB**	**MreBH**	**MreC**	**MreD**	**Pbp2A**
MSD alpha – No fit All traces, High velocity	1.24, *0.31*	1.21, *0.30*	1.22, *0.30*	1.21, *0.34*	1.29, *0.21*	1.31, *0.32*
MSD alpha – No fit Low velocity, All traces	0.41, *0.45*	0.41, *0.44*	0.43, *0.46*	0.44, *0.43*	0.57, *0.51*	0.46, *0.41*
MSD alpha, Fit > 0.95 **High velocity, Mfit > 0.95**	**1.44, *0.20***	**1.41, *0.19***	**1.41, *0.19***	**1.41, *0.17***	**1.42, *0.20***	**1.40, *0.21***
MSD alpha, Fit > 0.95 Low velocity, Mfit > 0.95	1.05, *0.17*	1.05, *0.17*	1.05, *0.18*	1.04, *0.14*	0.99, *0.13*	1.02, *0.14*

Angle of intersection to midline - Combined merodiploids and replacements						
All values in degrees	**Mbl**	**MreB**	**MreBH**	**MreC**	**MreD**	**Pbp2A**
Mean, *StdDev* **Traces RFit > 0.5**	***89.3, 27.0*** ***n=4615***	**90.2, *26.9*** ***n=2090***	**90.5, *36.2*** ***n=1276***	**89.7, *25.7*** ***n=1578***	**90.1, *25.7*** ***n=1097***	**89.5, *19.2*** ***n=2499***
- % within 15° of 90°	**68.5**	**68.3**	**57.1**	**70.7**	**69.6**	**84.3**
Mean, *StdDev* Traces RFit > 0.7	88.9*, 24.6* *n=1888*	90.7, *23.8* *n=787*	92.1, *31.9* *n=420*	89.7, *22.7* *n=887*	88.5, *23.3* *n=827*	89.2, *14.5* *n=1351*
- % within 15° of 90°	74.0	75.3	64.8	75.6	73.8	89.7
Angle of intersection to midline - Replacements						
	Mbl	**MreB**	**MreBH**	**MreC**	**MreD**	**Pbp2A**
Mean, *StdDev* All traces RFit > 0.5	90.8, *25.4* n=1437	89.9, *22.4* n=373	88.5, *18.7* n=203	89.6, *23.9* *n=1250*	90.2, *25.4* *n=955*	89.5, *17.5* *n=1995*
Mean, *StdDev* Traces RFit > 0.7	90.6, *25.0* n=687	89.9, *21.5* n=144	90.2, *14.6* n=64	89.3*, 22.5* n=792	88.4, *23.1* n=791	89.5, *13.6* n=1196
Angle of intersection to midline - Merodiploids						
	Mbl	**MreB**	**MreBH**	**MreC**	**MreD**	**Pbp2A**
Mean, *StdDev* Traces RFit > 0.5	88.7, *27.7* n=3178	90.3, *27.8* n=1717	90.8, *38.6* n=1073	89.4, *28.3* n=328	89.4, *28.4* n=142	89.5, *25.6* n=504
Mean, *StdDev* Traces RFit > 0.7	88.0, 24.3 n=1201	90.9, 24.3 n=643	92.4, 34.1 n=356	93.0, 24.3 n=95	90.2, 28.2 n=36	86.5, 19.9 n=155

Average length (distance traveled) - Merodiploids ***Note** - these measures do not represent the true distance particles travel *in vivo*, as cells were imaged with TIRF illumination, and most foci appear and disappear by entering or leaving the illumination plane.						
All values in nm	**Mbl**	**MreB**	**MreBH**	**MreC**	**MreD**	**Pbp2A**
Mean, *StdDev* **High velocity, Mfit >0.95**	359, *237*	336, *221*	255, *162*	440, *332*	393, *233*	413, *328*
Average length (distance traveled) - Replacements						
	Mbl	**MreB**	**MreBH**	**MreC**	**MreD**	**Pbp2A**
Mean, *StdDev* **High velocity, Mfit >0.95**	471, *324*	409, *234*	309, *158*	671, *427*	614, *453*	508, *355*

Table S3 - Plasmids used in this study

Plasmid	Description	Reference
pRB089	*yvbJ::PxylA-gfp-mreB (erm)*	This work
pRB087	*yvbJ::PxylA-gfp-pbp2A (erm)*	This work
pRB091	*yvbJ::PxylA-gfp-mreC (erm)*	This work
pRB092	*yvbJ::PxylA-gfp-mreD (erm)*	This work
pRB095	*rodZΩPspank-rodZ (cat)*	This work
pRB096	*rodAΩPspank-rodA (cat)*	This work
pRB105	*yhdG::Phyperspank-mreB (phleo)*	This work
pRB110	*yhdG::Phyperspank-mreB^{D158A} (phleo)*	This work
pRB111	*yhdG::Phyperspank-mreB^{E136A} (phleo)*	This work
pRB112	*yvbJ::PxylA-gfp-mreB^{D158A} (erm)*	This work
pRB113	*yvbJ::PxylA-gfp-mreB ^{E136A} (erm)*	This work
pRB115	*yhdG::Pspank-pbpA (phleo)*	This work
pRB117	*yhdG::PxylA-mCherry-mreB (phleo)*	This work
pDP309	*ΔmreB deletion plasmid*	Dan Kearns

Table S4 - Strains used in this study

Strain	Genotype	Source
BDR2061	*amyE::PxylA-gfp-mbl (spec), mblΩpMUTIN4 (erm), trpC2*	(*17*)
BDR2432	*mreBΩPxylA-gfp-mreB (cat)*	(*18*)
BDR2434	*mblΩPxylA-gfp-mbl (cat)*	(*18*)
BDR2435	*mreBHΩPxylA-gfp-mreBH (cat)*	(*18*)
BDR2436	*amyE::PxylA-gfp-mreB (spec)*	(*18*)
BDR2437	*amyE::PxylA-gfp-mbl (spec)*	(*18*)
BDR2438	*amyE::PxylA-gfp-mreBH (spec)*	(*18*)
BDR2444	*pbpAΩPxylA-gfp-pbpA (cat), trpC2*	(*19*)
BDR2447	*mreDΩPxylA-gfp-mreD (cat), trpC2*	(*20*)
BDR2448	*mreCΩPxylA-gfp-mreC (cat), trpC2*	(*20*)
BDR2450	*sinR::spec, epsA-O::tet, thrC::Peps-epsE-gfp (erm)*	(*21*)
BDR2452	*swrA+, sinR::spec, epsA-O::tet, thrC::Peps-epsE-gfp (erm)*	(*21*)
BDR2461	*ΔmreB, amyE::PxlyA-gfp-mbl (spec)*	This work
BDR2487	*pbpH::spec*	(*22*)
BDR2456	*pbpA::cat*	(*22*)
BRB684	*yvbJ::PxylA-gfp-pbp2A (erm)*	This work
BRB690	*yvbJ::PxylA-gfp-mreC (erm)*	This work
BRB692	*yvbJ::PxylA-gfp-mreD (erm)*	This work
BRB714	*rodAΩpRB096 [PspanK-rodA (cat)]*	This work
BRB718	*rodZΩpRB095 [PspanK-rodZ (cat)]*	This work
BRB728	*amyE::PxylA-gfp-mbl (spec), rodAΩpRB096 [PspanK-rodA (cat)]*	This work
BRB729	*amyE::Pxyl-gfp-mbl (spec), rodZΩpRB095 [PspanK-rodZ (cat)]*	This work
BRB736	*yvbJ::PxylA-gfp-mreB^{D158A} (erm)*	This work
BRB747	*amyE::PxylA-gfp-mbl (spec), yhdG::PhyperspanK-mreB^{D158A} (phleo)*	This work
BRB749	*sinR::kan, epsH::tet, mbl ΩPxylA-gfp-mbl (cat)*	This work
BRB755	*amyE::PxylA-gfp-mreB (spec), yhdG::PhyperspanK-mreB^{D158A} (phleo)*	This work
BRB757	*sinR::kan, epsH::tet, amyE::PxylA-gfp-mbl (spec)*	This work
BRB770	*yvbJ::PxylA-gfp-mreB^{E136A} (erm)*	This work
BRB781	*amyE::PxylA-gfp-mbl (spec), yhdG::PhypespanK-mreB^{E136A} (phleo)*	This work
BRB782	*amyE::PxylA-gfp-mreB (spec), yhdG::PhypespanK-mreB^{E136A} (phleo),*	This work
BRB783	*sinR::spec, epsA-O::tet, thrC::Peps-epsE-gfp (erm), yhdG::PxylA-mCherry-mreB (phleo)*	This work
BRB785	*yhdG::PspanK-pbpA (phleo), pbpH::spec, pbpA::erm, mbl ΩPxylA-gfp-mbl (cat)*	This work
BRB786	*yhdG::PspanK-pbpA (phleo), pbpH::spec, pbpA::cat, yvbJ::PxylA-gfp-mreB (erm)*	This work
BRB795	*ΔmreB, yvbJ::PxylA-gfp-mreB (erm)*	This work

Table S5 - Oligonucleotides used in this study

Primer	*Sequence*
oRB071	gcagGAATTCgtgccatgtc
oRB073	cgcGGATCCatCTCGAGatGCTAGCtcAAGCTTcattcaaatacagatgcattttat
oRB074	gccGCTAGCacataaggaggaactactatgagtaaaggagaagaacttttc
oRB075	ccgCTCGAGgcctgatcctttgtatagttcatccatgcc
oRB081	atattgaaaatactgacgagg
oRB082	aaataagtctagtgtgttagac
oRB085	cggCTCGAGatgtttggaattggtgctagag
oRB086	cgcGGATCcgtgttacacctcttctattg
oRB149	gccGCTAGCcagagaggaaaaagcaatg
oRB150	cgcGGATCCgttggcagcagctccagc
oRB151	gccGCTAGCaaggcgggatagaatgagtc
oRB152	cgcGGATCCaggtgcaatagactcggg
oRB157	cagGAATTCgactctctagc
oRB158	gccGCTAGCaattgttatccgctcacaattcc
oRB159	gccGCTAGCatGTCGACatACTAGTatggatccaagctaattcggtggaaacg
oRB160	ggcAAGCTTtaactcacattaattgcgttgcg
oRB161	ctgggattacacatggcatg
oRB163	gcgAAGCTTacataaggaggaactactatgtttggaattggtgctagag
oRB164	gccGCTAGCgtgttacacctcttctattgaac
oRB165	cgactggaagcatggttgttg**C**tatcgggggcggtacgac
oRB167	cgtacggtcaccgatcatcag
oRB173	gcgAAGCTTaggaagatacatacatatggtcagcaagggagagg
oRB174	cggCTCGAGgcctgatcctttgtataattcgtccattcc
oRB176	gcgAAGCTTaaatagaaaaggtgatgttatgagg
oRB177	ggcGCATGCgggtttgaaccgaatgttaagg
oRB182	cgattgctgcggcaaaaggc**G**cttcaatcggatacgcgtcac
oDR817	cggCTCGAGatgaggagaaataaaccaaaaaag
oDR818	cgcGGATCCgggtttgaaccgaatgttaag
oRB089	cggCTCGAGatgccgaataagcggttaatgc
oRB090	cgcGGATCCaagcatcataacgaaaggg
oRB091	cggCTCGAGgtgaaacgtttccttctccc
oRB092	cgcGGATcctcaacaacatactcatttcg
oDR829	catcaaatcttacaaatgtag
oDR830	actttatctacaaggtgtggc

Restriction endonuclease sites are capitalized.
MreB point mutations are in bold and capitalized.

Supplemental References

1. M. Bates, B. Huang, G. T. Dempsey, X. Zhuang, Multicolor super-resolution imaging with photo-switchable fluorescent probes. *Science* **317**, 1749 (Sep 21, 2007).
2. B. Huang, W. Wang, M. Bates, X. Zhuang, Three-dimensional super-resolution imaging by stochastic optical reconstruction microscopy. *Science* **319**, 810 (Feb 8, 2008).
3. O. Sliusarenko, J. Heinritz, T. Emonet, C. Jacobs-Wagner, High-throughput, subpixel precision analysis of bacterial morphogenesis and intracellular spatio-temporal dynamics. *Mol Microbiol* **80**, 612 (May, 2011).
4. K. P. Lemon, A. D. Grossman, Localization of bacterial DNA polymerase: evidence for a factory model of replication. *Science* **282**, 1516 (Nov 20, 1998).
5. E. Ricca, S. Cutting, R. Losick, Characterization of bofA, a gene involved in intercompartmental regulation of pro-sigma K processing during sporulation in Bacillus subtilis. *J Bacteriol* **174**, 3177 (May, 1992).
6. J. K. Wagner, K. A. Marquis, D. Z. Rudner, SirA enforces diploidy by inhibiting the replication initiator DnaA during spore formation in Bacillus subtilis. *Mol Microbiol* **73**, 963 (Sep, 2009).
7. H. J. Defeu Soufo, P. L. Graumann, Dynamic localization and interaction with other Bacillus subtilis actin-like proteins are important for the function of MreB. *Mol Microbiol* **62**, 1340 (Dec, 2006).
8. S. Vorobiev *et al.*, The structure of nonvertebrate actin: implications for the ATP hydrolytic mechanism. *Proc Natl Acad Sci U S A* **100**, 5760 (May 13, 2003).
9. E. C. Garner, C. S. Campbell, R. D. Mullins, Dynamic instability in a DNA-segregating prokaryotic actin homolog. *Science* **306**, 1021 (Nov 5, 2004).
10. J. A. Mayer, K. J. Amann, Assembly properties of the Bacillus subtilis actin, MreB. *Cell Motil Cytoskeleton* **66**, 109 (Feb, 2009).
11. R. E. Thompson, D. R. Larson, W. W. Webb, Precise nanometer localization analysis for individual fluorescent probes. *Biophys J* **82**, 2775 (May, 2002).
12. A. Yildiz *et al.*, Myosin V walks hand-over-hand: single fluorophore imaging with 1.5-nm localization. *Science* **300**, 2061 (Jun 27, 2003).
13. V. Levi, E. Gratton, Exploring dynamics in living cells by tracking single particles. *Cell Biochem Biophys* **48**, 1 (2007).
14. M. J. Saxton, K. Jacobson, Single-particle tracking: applications to membrane dynamics. *Annu Rev Biophys Biomol Struct* **26**, 373 (1997).
15. K. Jaqaman *et al.*, Robust single-particle tracking in live-cell time-lapse sequences. *Nat Methods* **5**, 695 (Aug, 2008).
16. A. Formstone, J. Errington, A magnesium-dependent mreB null mutant: implications for the role of mreB in Bacillus subtilis. *Mol Microbiol* **55**, 1646 (Mar, 2005).
17. R. Carballido-López, J. Errington, The bacterial cytoskeleton: in vivo dynamics of the actin-like protein Mbl of Bacillus subtilis. *Dev. Cell* **4**, 19 (Jan 1, 2003).

18. H. J. Defeu Soufo, P. L. Graumann, Dynamic movement of actin-like proteins within bacterial cells. *EMBO Rep* **5**, 789 (Aug, 2004).
19. D. J. Scheffers, L. J. Jones, J. Errington, Several distinct localization patterns for penicillin-binding proteins in Bacillus subtilis. *Mol Microbiol* **51**, 749 (Feb, 2004).
20. M. Leaver, J. Errington, Roles for MreC and MreD proteins in helical growth of the cylindrical cell wall in Bacillus subtilis. *Mol Microbiol* **57**, 1196 (Sep, 2005).
21. K. M. Blair, L. Turner, J. T. Winkelman, H. C. Berg, D. B. Kearns, A molecular clutch disables flagella in the Bacillus subtilis biofilm. *Science* **320**, 1636 (Jun 20, 2008).
22. Y. Wei, T. Havasy, D. C. McPherson, D. L. Popham, Rod shape determination by the Bacillus subtilis class B penicillin-binding proteins encoded by pbpA and pbpH. *J Bacteriol* **185**, 4717 (Aug, 2003).